CDF/TOP/DOC/CDFR/CDF10877
June 20, 2012
Version 1.0

Measurement of Top Dilepton Cross Section with CDF Full data using the DIL Selection

Chang-Seong Moon
University of Paris 7, Seoul National University

Aurore Savoy-Navarro
University of Paris 7, France

Soo-Bong Kim
Seoul National University, Korea

Hyunsoo Kim
Chuonbuk National University, Korea

Yen-Chu Chen
Fermi National Accelerator Laboratory; Institute of Physics, Academia Sinica, Taiwan

Andy Beretvas
Fermi National Accelerator Laboratory

Abstract

We report a measurement of the top pair production cross section with 9.1 fb^{-1} of CDF full data collected by CDF II detector. We use $t\bar{t}$ dilepton events selected and reconstructed with the di-lepton (DIL) event selection assuming $m_t = 172.5$ GeV/c^2. Signal selection and background estimates are based on the methods developed previously from earlier measurements [1].

$$\sigma_{t\bar{t}} = 7.66 \pm 0.46_{\text{stat}} \pm 0.66_{\text{syst}} \pm 0.47_{\text{lumi}} \text{ pb.}$$

for 625 pretag signal candidate events

$$\sigma_{t\bar{t}} = 7.47 \pm 0.50_{\text{stat}} \pm 0.53_{\text{syst}} \pm 0.46_{\text{lumi}} \text{ pb.}$$

for 254 tight SecVtx b-tagged signal candidate events

Contents

1 Introduction 3

2 Samples 3

3 Top DIL event selection 5

4 Cross Section Denominator 6
4.1 Check of Acceptance Corrections 7

5 Cross Section Numerator 15
5.1 N_{jet} scale factor 16
5.2 Diboson and DY/$Z \to \tau\tau$ backgrounds 16
5.3 Drell-Yan background 17
5.4 Fake Lepton background 19

6 Systematics Studies 35
6.1 Systematics due to PDF uncertainties 36

7 Background and Signal Tables 37
7.1 Pretag Signal Candidate events 37
7.2 b-tagged Signal Candidate events 47

8 Results 52

9 Conclusions 54

1 Introduction

This note reports on the measurement of the top cross section in the dilepton channel using centrally triggered electron and muon data corresponding to a luminosity of about 9.1 fb^{-1} (8.8 fb^{-1} with b-tagging), which is the full CDF RUN II data taken in between 2002 and 2011. We rely and build upon the signal selection and background estimate techniques developed for earlier measurements of the so-called top DIL cross section [1].

Section 2 reviews the data and MC samples used for the this analysis. Section 3 reviews the top DIL event selection. Section 4 explains how the DIL signal acceptance and cross-section denominator have been calculated. Section 5 reviews the inputs to the cross-section numerator, especially the background estimates. Section 6 reports on studies of the systematic uncertainties afflicting both signal and background. Background and signal expectations are reported in Section 7 and compared to the data. The cross section results for pretag and b-tagged DIL candidate events are shown in Section 8.

2 Samples

The results presented in this note are obtained by using full data collected by CDF in RUN II, and processed with version 6.1.6 of the CDF reconstruction software. For the MC samples, we use events generated with version 6.1.4mc patch "c" in the run range $141544 < \text{run} < 312510$, as well as samples generated with higher luminosity runs. Physics objects like electrons, muons, jets and missing transverse energy are as defined by the TopEventModule selection code [2] and saved in "topNtuple" format both for data and Monte Carlo events.

The data are collected either via the central high p_T electron (`bhelX`, where X = 0d, 0h, 0i, mi, mj, mk or mp) trigger paths, ELECTRON_CENTRAL_18 or muon (`bhmu0X`) trigger paths such as MUON_CMUP18 and MUON_CMX18.

We impose that the events pass the version 45 of the good run list, obtained with bits (1,1,4,1) including silicon run and (1,0,4,1) not including silicon run [3]. This version of the good run list, which includes partially recovered runs, ensures that the CDF detector was in good running condition both for CEM electrons and for CMUP muons. If good running conditions are required also for CMX muons, the luminosity of the samples is reduced slightly as reflected in Table. The good silicon requirement slightly reduces the luminosity of our samples and is used when a Phoenix plug electron is reconstructed in the event. The data samples used in this analysis are described in Table 1. We use "9.1 fb^{-1}" of data without good silicon run and "8.8 fb^{-1}" of data with good silicon run.

For Monte Carlo events, we use only events for runs in the good electron SI run list, i.e. obtained with bits (1,1,0,1). We also restrict any Monte Carlo acceptance calculation to events with run ≥ 150145, as the CMX detector was not fully functional before that time.

Data Sample	Run Range	Luminosity(pb^{-1}) without Silicon			Luminosity(pb^{-1}) with Silicon		
		CEM	CMUP	CMX	CEM/PHX	CMUP	CMX
Through p17	138425-261005	2825.95±169.56	2825.95±169.56	2760.39±165.62	2676.13±160.57	2676.13±160.57	2622.74±157.36
period 18	261119-264071	402.03 ± 24.12	392.72 ± 23.56	402.13 ± 24.13	397.35 ± 23.84	388.32 ± 23.30	397.46 ± 23.85
period 19	264101-266513	208.10 ± 12.49	208.10 ± 12.49	208.11 ± 12.49	206.98 ± 12.42	206.98 ± 12.42	206.99 ± 12.42
period 20	266528-267718	248.17 ± 14.89	248.15 ± 14.89	248.15 ± 14.89	226.92 ± 13.62	226.90 ± 13.61	226.90 ± 13.61
period 21	268155-271047	441.05 ± 26.46	441.03 ± 26.46	441.04 ± 26.46	435.59 ± 26.14	435.57 ± 26.13	435.58 ± 26.13
period 22	271072-272214	268.69 ± 16.12	268.69 ± 16.12	268.69 ± 16.12	265.67 ± 15.94	265.67 ± 15.94	265.67 ± 15.94
period 23	272470-274055	203.74 ± 12.22	203.77 ± 12.23	203.77 ± 12.23	200.65 ± 12.04	200.68 ± 12.04	200.68 ± 12.04
period 24	274123-275848	264.68 ± 15.88	264.70 ± 15.88	264.70 ± 15.88	252.06 ± 15.12	252.09 ± 15.13	252.09 ± 15.13
period 25	275873-277511	227.37 ± 13.64	227.37 ± 13.64	227.37 ± 13.64	211.47 ± 12.69	211.47 ± 12.69	211.47 ± 12.69
period 26	282976-284843	170.79 ± 10.25	170.78 ± 10.25	170.79 ± 10.25	163.86 ± 9.83	163.85 ± 9.83	163.86 ± 9.83
period 27	284858-287261	402.21 ± 24.13	402.21 ± 24.13	402.21 ± 24.13	397.62 ± 23.86	397.62 ± 23.86	397.62 ± 23.86
period 28	287294-289197	266.01 ± 15.96	266.01 ± 15.96	266.01 ± 15.96	261.15 ± 15.67	261.15 ± 15.67	261.15 ± 15.67
period 29	289273-291025	305.84 ± 18.35	305.84 ± 18.35	305.84 ± 18.35	291.25 ± 17.48	291.25 ± 17.48	291.25 ± 17.48
period 30	291294-293800	449.16 ± 26.95	449.16 ± 26.95	449.16 ± 26.95	422.38 ± 25.34	422.38 ± 25.34	422.38 ± 25.34
period 31	293826-294777	149.78 ± 8.99	149.78 ± 8.99	149.78 ± 8.99	138.46 ± 8.31	138.46 ± 8.31	138.46 ± 8.31
period 32	294778-299367	430.12 ± 25.81	431.58 ± 25.89	431.58 ± 25.89	420.66 ± 25.24	422.08 ± 25.24	422.08 ± 25.24
period 33	299368-301303	376.10 ± 22.57	376.10 ± 22.57	376.10 ± 22.57	363.88 ± 21.83	363.88 ± 21.83	363.88 ± 21.83
period 34	301952-303853	290.05 ± 17.40	290.05 ± 17.40	290.05 ± 17.40	286.06 ± 17.16	286.06 ± 17.16	286.06 ± 17.16
period 35	304269-306762	330.28 ± 19.82	330.28 ± 19.82	330.28 ± 19.82	328.04 ± 19.68	328.04 ± 19.68	328.04 ± 19.68
period 36	306791-308554	403.99 ± 24.24	403.99 ± 24.24	403.99 ± 24.24	399.56 ± 23.97	399.56 ± 23.97	399.56 ± 23.97
period 37	308570-310441	174.15 ± 10.45	174.15 ± 10.45	174.15 ± 10.45	173.50 ± 10.41	173.50 ± 10.41	173.50 ± 10.41
period 38	310472-312510	246.46 ± 14.79	246.46 ± 14.79	246.46 ± 14.79	243.89 ± 14.63	243.89 ± 14.63	243.89 ± 14.63
Total	138425-312510	9084.68±545.08	9076.87± 544.61	9020.75±541.25	8763.13±525.79	8755.53±525.33	8711.31±522.68

Table 1: Run ranges and luminosity for various data taking periods. All of the above luminosities includes the correction factor of 1.019 ± 0.060 [5].

The cross sections for SM processes that we consider as backgrounds and which can be simulated in a MC are given in Table 2. The main $t\bar{t}$ signal MC sample is the 6.72 M events of inclusive PYTHIA 1.884 sample generated at $M_{top} = 172.5$ GeV (`ttop25`). In this case, we simulate events up to run 259614, which match the maximum run number accepted for the data. To model the main sources of Standard Model backgrounds to the top dilepton channel we use:

- ALPGEN+PYTHIA `all` $Z(ee)$ `sample` for DY/$Z \to ee$
- ALPGEN+PYTHIA `all` $Z(\mu\mu)$ `sample` for DY/$Z \to \mu\mu$
- ALPGEN+PYTHIA `all` $Z(\tau\tau)$ `sample` for DY/$Z \to \tau\tau$
- `ihht1a/jhht1a/khht1a` for $WW/WZ/ZZ$ diboson events

Process	Cross Section σ (pb)	K-factor
WW	11.34±0.68	NA
WZ	3.47±0.21	NA
ZZ	3.62±0.22	NA
W($\rightarrow e\nu$)γ	32±3.2	1.36
W($\rightarrow \mu\nu$)γ	32±3.2	1.34

Table 2: Cross Sections for different Standard Model processes considered as background to the top DIL selection. The final NLO cross section are either already quote here as σ or obtained multiplying the σ in the first column by the K-factor in the second column.

- `rewk28/rewk29` for $W\gamma$, $W \rightarrow e\nu/W \rightarrow \mu\nu$ events

All of the backgrounds are generated with PYTHIA 6.216, with the exception of the Wγ samples which are generated with the Baur Monte Carlo. We used the ALPGEN+PYTHIA DY/Z samples are generated for $M_{\ell\ell} > 8$ GeV. The ZZ events are generated with $M_{\ell\ell} > 2$ GeV. Their cross section is obtained by multiplying a NLO MCFM calculation for $M_{\ell\ell} > 15$ GeV of 2.1 pb [4] by the fraction of events found with $M_{\ell\ell} <$ 15 GeV over the total. A 20% uncertainty is assumed for $\sigma(ZZ)$ given the uncertainty of the extrapolation method. Table 2 summarizes the NLO cross sections assumed for each MC sample.

The calculation of events with one jet/track faking a lepton uses fake lepton identification rates extracted to the JET50 inclusive jet samples `gjt20X`, where X = d, h, i, j, k or m. Fake rates from the JET20 (`gjt10X`), JET70 (`gjt30X`) and JET100 (`gjt40X`) samples are used to access the systematic uncertainty on the fake estimates.

3 Top DIL event selection

DIL selection aims at reconstructing $t\bar{t}$ events with both W's from top decaying leptonically. It requires two fully identified electrons or muons with transverse energy above 20 GeV, $\not\!\!E_T > 25$ GeV and at least two tight jets of $E_T > 15$ GeV. Two additional selection criteria are added, which are dilepton invariant mass > 5 GeV for Monte Calro cannot describile in this region and COT radius exit cut > 140 cm for CMIO due to removal simulation mis-modeling events around the end of COT. The first, or trigger lepton can be one of three types: CEM electron, CMUP or CMX muon. The second, or loose lepton, can be also non-isolated or an isolated PHX electron or one of the non-trigger muon types: CMU-only, CMP-only and CMIO. Details on the cuts used to identify each lepton category are contained in [6]. Non isolated counterpart of the trigger leptons (i.e. NICEM electrons and NICMUP/NICMX muons) are allowed to trigger the event when they come together with a PHX electron to recover most of the acceptance lost by dropping the plug electron dataset.

The jets are corrected up to hadron level (i.e. up to Level 5) using version "JetCorr19" of the JetUser module. The "Multiple Interactions" or level 4 jet correction is applied to each event on the basis of the number of good (i.e. quality 12 or higher) z-vertexes in the event. We should mention here that for the purpose of correcting $\not\!\!E_T$ (which is calculated starting from the raw transverse energy deposited in each tower of the calorimeter), we used the jet energy scale calculated ignoring the level 4 correction in order to avoid over-correcting $\not\!\!E_T$ for the presence of energy due to extra interactions.

Extra event topology cuts are imposed to improve the purity of the selection:

- Dilepton invariant mass > 5 GeV.
- COT radius exit cut > 140 cm for CMIO due to removal simulation mis-modeling events around the end of COT.
- Z-veto for ee and $\mu\mu$ events with reconstructed dilepton invariant mass in the 76-106 GeV window. See details below.
- L-cut in the ($\not\!\!E_T$, $\delta\phi_{min}$) plane to reject Z$\rightarrow$ $\tau\tau$ events and events with mis-measured $\not\!\!E_T$ from jets pointing to cracks in the calorimeter: this cut requires the event $\not\!\!E_T$ to be above 50 GeV if there is any lepton or jet inside 20° of the $\not\!\!E_T$ direction.
- H$_T$ > 200 GeV cut to suppress events from an initial state lighter that $t\bar{t}$
- opposite charge for the two leptons.

We use the Z-veto cut which requires the minium significance of the missed transverse energy in the event. We defined MET Significance as:

$$MetSig = \frac{\not\!\!E_T}{\sqrt{E_T^{sum}}} \tag{1}$$

where E_T^{sum} is the sum of transverse raw energies deposited in all calorimeter towers, corrected for any muon P$_T$ and for the difference between the raw and the non-lv4 corrected energy of tight jets in the event. We find that a cut on $MetSig > 4\sqrt{\mathrm{GeV}}$ reduce the background by $\sim$ 25%, mostly in the Drell-Yan channel and reject $\sim$ 5% of the $t\bar{t}$ events.

4 Cross Section Denominator

The denominator of the cross section calculation can be written as an acceptance times the luminosity (see section 4 of CDF-8040). The acceptance itself is the convolution of the MC acceptance and of different correction factors estimated from comparing the efficiency predicted by MC and data in independent control samples. For the DIL selection we choose to compute the denominator as:

$$\begin{aligned}\mathcal{A}\times\mathcal{L} &= \sum_i \mathcal{A}_i \times \mathcal{L}_i \\ \mathcal{A}_i &= \mathcal{A}_{\ell_1\ell_2}\times C_{\ell_1\ell_2}\end{aligned} \quad (2)$$

where the index i run over all of the DIL selection categories, each made of a pair of leptons, $\ell_1\ell_2$. The PYTHIA $t\bar{t}$ MC raw efficiencies efficiencies $A_{\ell_1\ell_2}$, calculated as the ratio of the number of dilepton events passing the DIL selection in the `ttop25` MC sample, are multiplied by the dilepton correction factors $C_{\ell_1\ell_2}$ and by the luminosities $\mathcal{L}_i$ appropriate for each lepton pair.

The dilepton correction factors $C_{\ell_1\ell_2}$ are calculated using the following factorization.

$$C_{\ell_1\ell_2} = \epsilon_{z_0}\times(\epsilon_{trg_1}+\epsilon_{trg_2}-\epsilon_{trg_1}\epsilon_{trg_2})\times SF_1 SF_2 \quad (3)$$

where ϵ_{z_0} is efficiency of the cut imposed on all MC events to have the event vertex reconstructed inside a $\pm$60 cm region from the nominal z=0; ϵ_{trg_i} are the trigger efficiencies for the two leptons; SF_i are the identification scale factor, measured as the ratios of the data over the MC lepton identification and muon reconstruction efficiencies.

The trigger efficiencies and identifcation scale factors for each single lepton in the dilepton pair are reported in Table 3. The central value used for each term is the luminosity weighted average of different values measured for the 0d, 0h, 0i, mi, mj, mk and mm periods, as listed in the table. The efficiency of the event for the primary vertex $|z_{VTX}| < 60$ cm cut is also reported in Table 3.

Table 4 details all of the inputs to equation 2. The total acceptance for the pretag candidate dilepton events is $\mathcal{A}$=0.7558 $\pm$ 0.0035% and for the b-tagged events is $\mathcal{A}$=0.4610 $\pm$ 0.0027%. A validation of the factorization model used for $C_{\ell_1\ell_2}$ is obtained by measuring the Z boson cross section for each dielectron and dimuon category. Section 4.1 reports on the results of this validation.

Summing over all of the DIL categories, we obtain a denominator for the 9.1 fb^{-1}DIL cross section of 55.7540 $\pm$ 0.2581 pb^{-1} for pretag and 31.7031 $\pm$ 0.1872 pb^{-1} for b-tagging, where the uncertainty comes solely from the propagation of the uncertainties of each term in equation 3.

4.1 Check of Acceptance Corrections

As a cross-check of our lepton selection, as well as the quoted luminosities, trigger efficiencies and scale factors used in final calculation of $t\bar{t}$ cross section, we measure the cross section of on-shell Z production.

We select the events which have ee or $\mu\mu$ pair in the final state. Cosmic events and events with an identifies conversions are removed. We required the two leptons to have opposite charges and invariant mass in the range 76 GeV/c^2 to 106 GeV/c^2.

Lepton Type	Vertex Reconstruction efficiency ϵ_{z_0}	
	5.1 fb^{-1}	9.1 fb^{-1}
All	0.9711 $\pm$ 0.0003	0.9747 $\pm$ 0.0002

Lepton Type	PHX charge fake rate	
	5.1 fb^{-1}	9.1 fb^{-1}
PHX	1.0065 $\pm$ 0.0016	1.0073 $\pm$ 0.0012

Lepton Type	Trigger efficiency ϵ_{trg}	
	5.1 fb^{-1}	9.1 fb^{-1}
CEM	0.9627 $\pm$ 0.0007	0.9544 $\pm$ 0.0006
CMUP	0.9151 $\pm$ 0.0014	0.9084 $\pm$ 0.0011
CMX	0.8906 $\pm$ 0.0018	0.8684 $\pm$ 0.0017

Lepton Type	Lepton Identification Scale Factor SF	
	5.1 fb^{-1}	9.1 fb^{-1}
CEM	0.9760 $\pm$ 0.0011	0.9739 $\pm$ 0.0009
NICEM	0.9848 $\pm$ 0.0010	0.9828 $\pm$ 0.0009
PHX	0.9205 $\pm$ 0.0019	0.9080 $\pm$ 0.0015
CMUP	0.8974 $\pm$ 0.0017	0.8691 $\pm$ 0.0013
NICMUP	0.9070 $\pm$ 0.0015	0.8851 $\pm$ 0.0012
CMX	0.9564 $\pm$ 0.0017	0.9347 $\pm$ 0.0015
NICMX	0.9640 $\pm$ 0.0015	0.9502 $\pm$ 0.0013
CMU	0.8922 $\pm$ 0.0035	0.8841 $\pm$ 0.0027
NICMU	0.9020 $\pm$ 0.0032	0.8997 $\pm$ 0.0024
CMP	0.8867 $\pm$ 0.0031	0.8594 $\pm$ 0.0024
NICMP	0.8962 $\pm$ 0.0028	0.8745 $\pm$ 0.0022
CMIO	1.0323 $\pm$ 0.0033	1.0199 $\pm$ 0.0026

Table 3: List by lepton type of vertex reconstruction efficiency ϵ_{z_0}, PHX charge fake rate, trigger efficiency ϵ_{trg}, and lepton identification scale factors SF. For lepton types labelled with a NI means non isolated leptons only.

The acceptance is calculated using DY/Z $\rightarrow$ ee and $\mu\mu$ PYTHIA Monte Carlo samples. The MC acceptance is defined by the number of events which pass the selection described above, divided by the number of events in which invariant mass of two leptons satisfies 76 GeV/c^2 < $M_{\ell\ell}$ < 106 GeV/c^2.

Since the CMX trigger rate is changed with jet requiremnet from run number 226194 in the dataset period 9 to run number 257201 in the period 16. we use two different kind of the CMX trigger for 0jet control bin and 1 jet or more than 1 jet bin. For 0jet bin we use the inclusive high p_T CMX trigger such as MUON_CMX18_DPS or MUON_CMX18_L2_LOOSE_DPS or MUON_CMX18_L2_LOOSE_LUMI_200 or MUON _CMX18_LUMI_250. Meanwhile for 1 jet or more jets, the CMX trigger with JET10 for

Category	$\mathcal{A}_{\ell_1\ell_2}(\%)$	$C_{\ell_1\ell_2}$	$\mathcal{L}_i(\mathrm{pb}^{-1})$
CEM-CEM	0.0958 $\pm$ 0.0012	0.9203 $\pm$ 0.0018	9084.68
CEM-NICEM	0.0202 $\pm$ 0.0006	0.9291 $\pm$ 0.0012	9084.68
PHX-CEM	0.0404 $\pm$ 0.0008	0.8247 $\pm$ 0.0017	8763.13
PHX-NICEM	0.0036 $\pm$ 0.0002	0.8325 $\pm$ 0.0017	8763.13
CMUP-CMUP	0.0364 $\pm$ 0.0008	0.7296 $\pm$ 0.0022	9076.87
CMUP-NICMUP	0.0094 $\pm$ 0.0004	0.7429 $\pm$ 0.0015	9076.87
CMUP-CMU	0.0159 $\pm$ 0.0005	0.7089 $\pm$ 0.0025	9076.87
CMUP-NICMU	0.0020 $\pm$ 0.0002	0.7214 $\pm$ 0.0023	9076.87
CMUP-CMP	0.0222 $\pm$ 0.0006	0.6325 $\pm$ 0.0022	9076.87
CMUP-NICMP	0.0028 $\pm$ 0.0002	0.6436 $\pm$ 0.0021	9076.87
CMUP-CMX	0.0382 $\pm$ 0.0008	0.7855 $\pm$ 0.0017	9020.75
CMUP-NICMX	0.0040 $\pm$ 0.0002	0.7977 $\pm$ 0.0016	9020.75
CMX-NICMUP	0.0042 $\pm$ 0.0003	0.7998 $\pm$ 0.0016	9076.87
CMUP-CMIO	0.0140 $\pm$ 0.0005	0.7701 $\pm$ 0.0025	9076.87
CMX-CMX	0.0092 $\pm$ 0.0004	0.8442 $\pm$ 0.0025	9020.75
CMX-NICMX	0.0015 $\pm$ 0.0002	0.8574 $\pm$ 0.0017	9020.75
CMX-CMU	0.0067 $\pm$ 0.0003	0.7321 $\pm$ 0.0028	9020.75
CMX-NICMU	0.0006 $\pm$ 0.0001	0.7450 $\pm$ 0.0026	9020.75
CMX-CMP	0.0103 $\pm$ 0.0004	0.6532 $\pm$ 0.0025	9020.75
CMX-NICMP	0.0011 $\pm$ 0.0001	0.6646 $\pm$ 0.0024	9020.75
CMX-CMIO	0.0062 $\pm$ 0.0003	0.7953 $\pm$ 0.0028	9020.75
CEM-CMUP	0.1337 $\pm$ 0.0014	0.8203 $\pm$ 0.0015	9076.87
CEM-NICMUP	0.0185 $\pm$ 0.0005	0.8353 $\pm$ 0.0014	9076.87
CMUP-NICEM	0.0139 $\pm$ 0.0005	0.8282 $\pm$ 0.0014	9076.87
CEM-CMU	0.0299 $\pm$ 0.0007	0.8343 $\pm$ 0.0026	9084.68
CEM-NICMU	0.0034 $\pm$ 0.0002	0.8490 $\pm$ 0.0024	9084.68
CEM-CMP	0.0409 $\pm$ 0.0008	0.7443 $\pm$ 0.0024	9084.68
CEM-NICMP	0.0055 $\pm$ 0.0003	0.7574 $\pm$ 0.0022	9084.68
CEM-CMX	0.0677 $\pm$ 0.0010	0.8848 $\pm$ 0.0016	9020.75
CEM-NICMX	0.0080 $\pm$ 0.0004	0.8986 $\pm$ 0.0014	9020.75
CMX-NICEM	0.0060 $\pm$ 0.0003	0.8932 $\pm$ 0.0015	9020.75
CEM-CMIO	0.0240 $\pm$ 0.0006	0.9063 $\pm$ 0.0026	9020.75
PHX-CMUP	0.0282 $\pm$ 0.0007	0.7008 $\pm$ 0.0018	8755.53
PHX-NICMUP	0.0030 $\pm$ 0.0002	0.7135 $\pm$ 0.0018	8755.53
PHX-CMX	0.0128 $\pm$ 0.0004	0.7237 $\pm$ 0.0022	8711.31
PHX-NICMX	0.0014 $\pm$ 0.0001	0.7350 $\pm$ 0.0021	8711.31

Table 4: List, by dilepton category, of raw acceptance $\mathcal{A}_{\ell_1\ell_2}$, correction factor $C_{\ell_1\ell_2}$ and luminosity $\mathcal{L}_i$ used to calculate the denominator for the 9.1 fb^{-1} DIL cross section measurement. The raw acceptance uncertainty comes purely from the MC statistics. The error in the $C_{\ell_1\ell_2}$ comes from the propagation of the single lepton efficiency uncertainties reported in Table 3. "NI" means non-isolated leptons only.

top quark such as MUON_CMX18_&_JET10 or MUON_CMX18_&_JET10_LUMI_270 or MUON_CMX18_&_JET10_DPS are used.

We use the inclusive CMX trigger for Z cross section measurement. The measured on-shell Z cross sections are shown in Figure 2, 3, 4 for the $Z \to ee$, $Z \to$ CMUP-any μ and $Z \to$ CMX-any μ channels respectively. We show the Z cross section as a function of run range to check for any time dependence of the overall scale factors. The error bar in the figures reflects uncertainties of data statistics, MC statistics and overall scale factors. The measured on-shell Z cross sections over the whole 9.1 fb^{-1} data sample are shown in Table 5 and Figure 1.

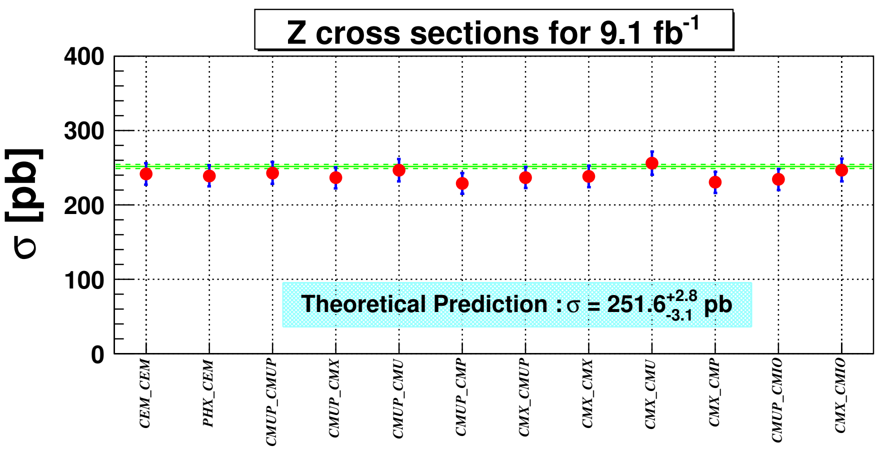

Figure 1: A summary of the measured Z cross sections of inclusive dilepton category in 9.1 fb^{-1}. The red line means statistical and systematic error and the blue line shows total error including luminosity error.

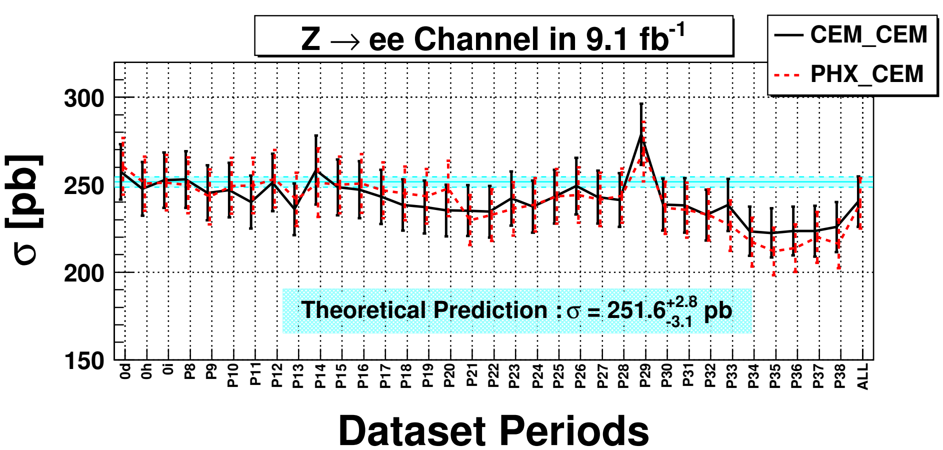

Figure 2: Z cross section before applying additional scale factor using Z→ ee channel as a function of run period. “P8” ∼ “P38” means the data from Period 8 until Period 38.

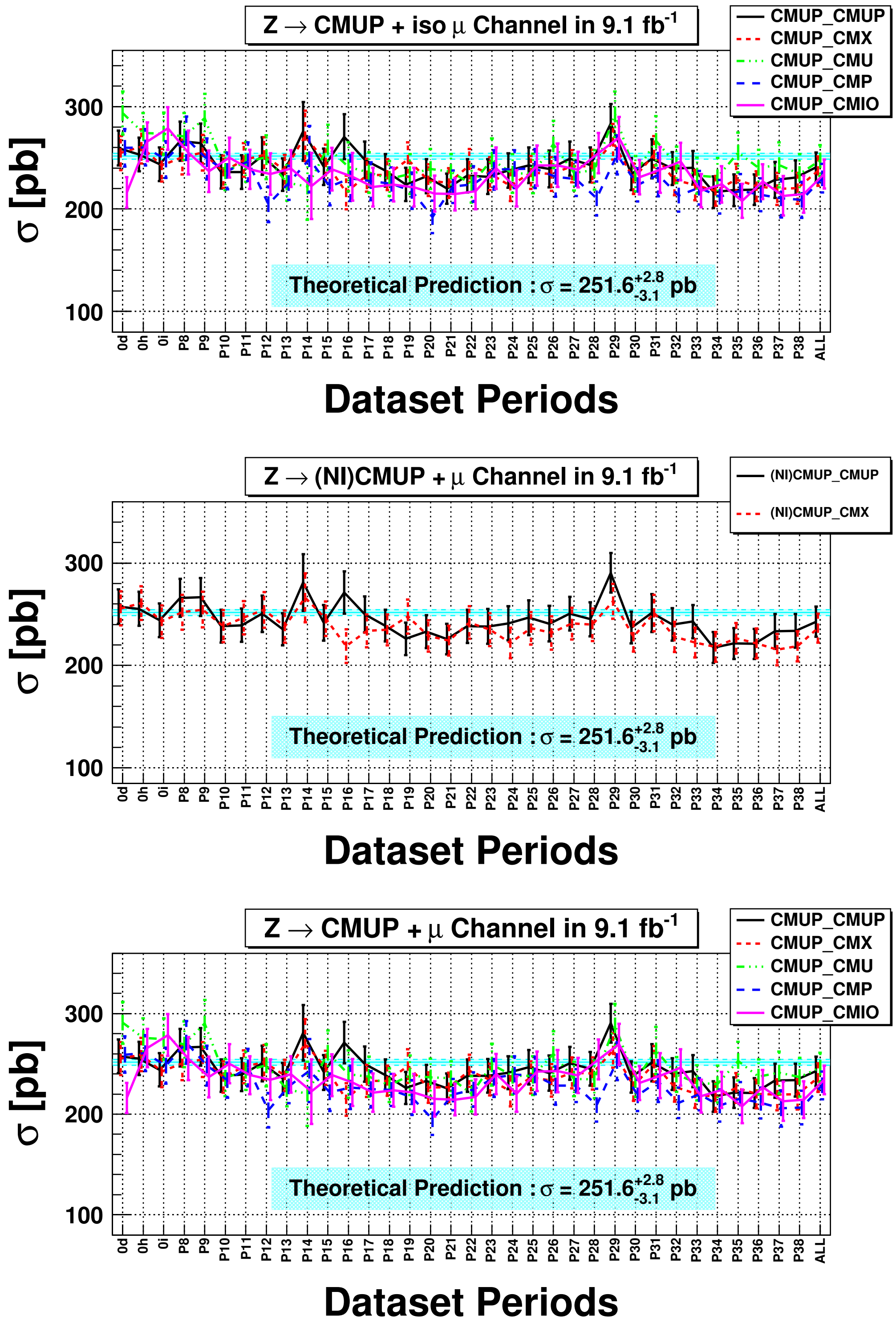

Figure 3: Z cross section before applying additional scale factor using Z→ CMUP-any μ channel as a function of run period. "NI" means inclusive, i.e. both isolated and non-isolated leptons are included.

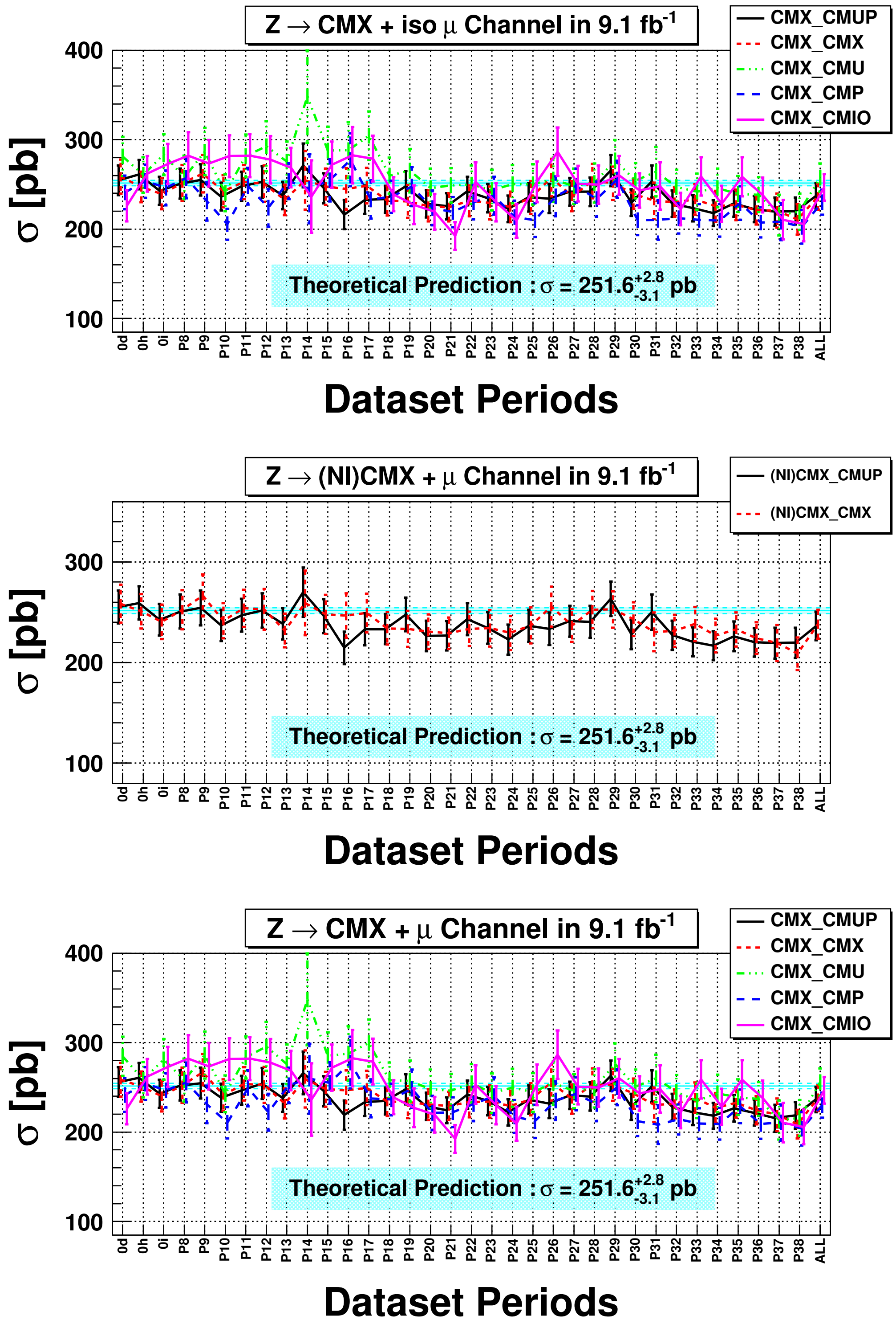

Figure 4: Z cross section before applying additional scale factor using Z→ CMX-any μ channel as a function of run period. “NI” means inclusive, i.e. both isolated and non-isolated leptons are included.

Category	Z Cross Section (pb) Original	Fitted
CEM-CEM	240.4 ± 14.4	240.4 ± 14.4
CEM-(NI)CEM	241.3 ± 14.5	241.3 ± 14.5
PHX-CEM	239.4 ± 14.4	239.4 ± 14.4
CEM-(NI)PHX	238.9 ± 14.4	238.9 ± 14.4
CMUP-CMUP	240.7 ± 14.5	240.7 ± 14.5
CMUP-(NI)CMUP	242.7 ± 14.6	242.7 ± 14.6
CMUP-CMU	247.4 ± 15.0	237.2 ± 14.4
CMUP-(NI)CMU	246.3 ± 14.9	236.1 ± 14.3
CMUP-CMP	230.1 ± 13.9	240.8 ± 14.6
CMUP-(NI)CMP	228.6 ± 13.8	239.2 ± 14.5
CMUP-CMIO	234.1 ± 14.2	235.0 ± 14.2
CMUP-CMX	237.1 ± 14.3	237.1 ± 14.3
CMUP-(NI)CMX	236.2 ± 14.2	236.2 ± 14.2
CMX-(NI)CMUP	236.5 ± 14.2	236.5 ± 14.2
CMX-CMX	236.2 ± 14.3	236.2 ± 14.3
CMX-(NI)CMX	238.1 ± 14.4	238.1 ± 14.4
CMX-CMU	257.6 ± 15.7	246.9 ± 15.0
CMX-(NI)CMU	255.8 ± 15.6	245.3 ± 14.9
CMX-CMP	229.9 ± 14.0	240.6 ± 14.6
CMX-(NI)CMP	230.1 ± 14.0	240.8 ± 14.6
CMX-CMIO	246.7 ± 15.0	247.6 ± 15.1

Table 5: The original and the fitted Z cross section in 9.1 fb^{-1} for the different ee and $\mu\mu$ dilepton categories with dilepton invariant mass in the range 76 GeV/c^2 to 106 GeV/c^2. (NI) means inclusive, i.e. both isolated and non-isolated leptons are included.

The categories with two tight leptons (CEM-CEM, CEM-PHX, CMUP-CMUP, CMUP-CMX and CMX-CMX), which are also the ones with the largest acceptance, are consistent with the theoretical prediction of $251.6^{+2.8}_{-3.1}$ pb [7]. Categories with a loose muon (CMP, CMU or CMIO) paired to a tight muon show some residual variation around the average value which is not consistent with statistical fluctuations. In order to find a consistent normalization for all data, we perform a fit to the Z cross sections in the different dilepton categories with three free parameters, corresponding to a multiplicative factor in front of the selection efficiency of each of the three loose muon categories. The fit returns the cross sections reported in the last column of Table 5 and an average Z peak cross section of 239.8 ± 14.4 pb, as shown in Figure 1.

Lepton Type	Lepton Identification Scale Factor SF	
	5.1 fb^{-1}	9.1 fb^{-1}
CMUP	0.8974 $\pm$ 0.0017	0.8691 $\pm$ 0.0013
NICMUP	0.9070 $\pm$ 0.0015	0.8851 $\pm$ 0.0012
CMX	0.9564 $\pm$ 0.0017	0.9347 $\pm$ 0.0015
NICMX	0.9640 $\pm$ 0.0015	0.9502 $\pm$ 0.0013
CMU	0.9386 $\pm$ 0.0035	0.9222 $\pm$ 0.0027
NICMU	0.9489 $\pm$ 0.0032	0.9385 $\pm$ 0.0024
CMP	0.8609 $\pm$ 0.0031	0.8213 $\pm$ 0.0024
NICMP	0.8702 $\pm$ 0.0028	0.8358 $\pm$ 0.0022
CMIO	0.9982 $\pm$ 0.0033	1.0163 $\pm$ 0.0026

Table 6: After applying the additional scale factors, lepton identification scale factors SF.

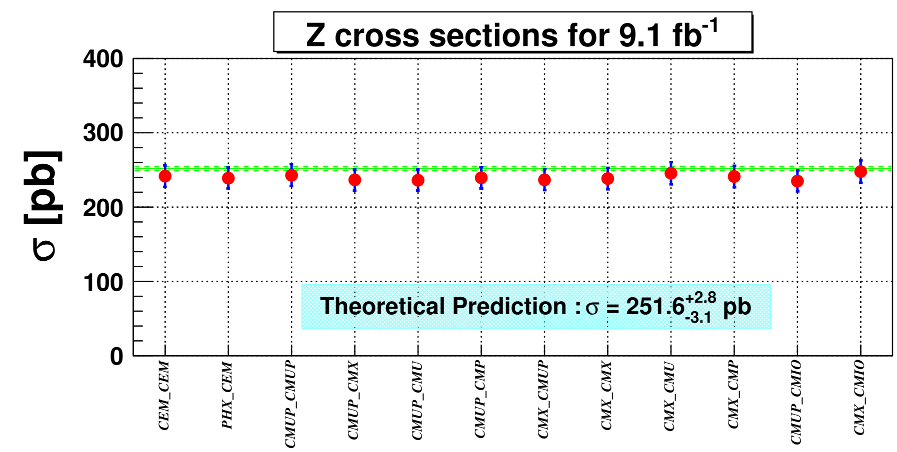

Figure 5: A summary of the fitted Z cross sections of inclusive dilepton category in 9.1 fb^{-1} . The red line means statistical and systematic error and the blue line shows total error including luminosity error.

The free parameters returned by the fit are: $\mathrm{SF}^{Z}_{\mathrm{CMP}} = 0.9557 \pm 0.0059$, $\mathrm{SF}^{Z}_{\mathrm{CMU}} = 1.0431 \pm 0.0074$ and $\mathrm{SF}^{Z}_{\mathrm{CMIO}} = 0.99641 \pm 0.0069$. They are folded into the acceptance correction procedure as additional scale factors to be multiplied by the lepton identification scale factors of Table 3 for the appropriate categories. After the fit, using the new lepton identification scale factors are shown in Table 6, the single Z cross section measurements are consistent with each other within uncertainties, with the possible exception of categories containing one CMIO loose muon for which we observe a maximum deviation equal to 10% of the average value in Figure 5. This systematic deviation affects only 10% of the DIL $t\bar{t}$ raw acceptance, corresponding to the summed contributions of any dilepton pair containing a CMIO muon in Table 4. Therefore we estimate a final 1% systematic uncertainty on the acceptance due to the correction procedure. We add this 1% uncertainty into the lepton ID sytematic uncertainty.

5 Cross Section Numerator

The numerator of the top dilepton DIL cross section is calculated as the difference between the total number of events found passing the DIL selection cuts in the data and the total background contamination expected from known Standard Model sources and fakes.

The background contamination is estimated following the methods used in CDF-8040. We can divide the backgrounds in two broad categories: MC-based and data-based. In the first category we include backgrounds coming from Standard Model processes with low cross sections, such as diboson decays, or with final state signatures for which it is hard to define an independent data control sample, as it is the case for DY/$Z \to \tau\tau$ events. For these sources of Standard Model events, we use the MC samples described in Section 2. The number of events passing the DIL selection is corrected by the factors $C_{\ell_1\ell_2} \times \mathcal{L}_i$ listed in Table 4, and normalized to the NLO cross sections of Table 2.

In the second category we include background contamination coming from hard to model detector effects, like lepton contamination from jets and fake $\not\!\!E_T$. These two effects, although small in magnitude, generate background events with two leptons in the final state because they tap onto large cross section processes like W+jets with a real lepton+$\not\!\!E_T$ from the W decay and a fake lepton from a jet, and DY/Z+jets with two real leptons and $\not\!\!E_T$ from mis-measured jet activity.

Our strategy for validating the background estimation is to compare data and background estimates in the so-called 0-jet and 1-jet bins. These control data samples come from events with two identified leptons passing all of the cuts applied to the top DIL candidate sample, except for the requirement of at least 2 tight jets and $\mathrm{H}_T > 200$ GeV. The low number of jets greatly limit the $t\bar{t}$ contribution and so they naturally provide a control sample of events sharing most of the DIL candidates kinematic signatures and very little signal contamination.

New for this version of the DIL selection is the inclusion of two new diboson processes besides the WW and WZ processes already considered in the past. We considered possible contaminations from ZZ events, with one Z decaying leptonically and the other hadronically, and from $W\gamma$ events, with the W decaying leptonically and the photon conversion providing the second lepton. Both are found to contribute very little to the $\geq$ 2jet sample but non negligible amounts to the 0-jet and 1-jet control bins.

Finally, the estimate of DY/$Z \to ee$ and $\mu\mu$ events has been improved with respect to the method used in past analysis both by relying less on MC estimates and by using control regions less affected by the $t\bar{t}$ contribution. More details on the new calculation are in Section 5.3.

5.1 N_{jet} scale factor

Since Monte Carlo does not model properly the jet multiplicity spectrum of events with jets from ISR and FSR radiation, we correct the fraction of Monte Carlo events with no prompt jets (i.e WW, Wγ and DY/$Z \to \tau\tau$) reconstructed in the 0, 1 and $\geq$ 2-jet bins by the correction factors C_{0j}, C_{1j} and C_{2j}, also called N_{jet} scale factors. These factors for WW, Wγ background are calculated by comparing data and PYTHIA MC predictions for the jet multiplicity of ee and $\mu\mu$ events in the Z-window region. On the other hand, we compare data and Alpgen MC prediction for DY/$Z \to \tau\tau$ background. In the Table 7 the top table shows the N_{jet} scale factors for WW and $W\gamma$ background, calculated using the PYTHIA Monte Carlo sample and the bottom table lists the scale factor of DY/Z background using the ALPGEN+PYTHIA Monte Carlo sample.

	N_{jet} Scale Factor for WW, Wγ		
	ee	$\mu\mu$	All
C_{0j}	1.016 ± 0.002	1.017 ± 0.003	1.016 ± 0.002
C_{1j}	0.922 ± 0.004	0.918 ± 0.006	0.920 ± 0.004
C_{2j}	1.032 ± 0.009	1.057 ± 0.011	1.042 ± 0.008

	N_{jet} Scale Factor for DY/Z		
	ee	$\mu\mu$	All
C_{0j}	0.991 ± 0.003	1.001 ± 0.004	0.995 ± 0.003
C_{1j}	1.020 ± 0.005	0.985 ± 0.006	1.006 ± 0.004
C_{2j}	1.098 ± 0.009	1.047 ± 0.012	1.076 ± 0.007

Table 7: Jet fraction correction factors for the 0, 1 and $\geq$ 2-jet bins for $Z \to ee$ and $Z \to \mu\mu$ events. The last column is the weighted average of the two dilepton Z samples and it is used for eμ reconstructed events. (The error is only statistical. Systematic error is added by 5 %)

5.2 Diboson and DY/$Z \to \tau\tau$ backgrounds

The number of diboson and DY/$Z \to \tau\tau$ background events selected at different steps of the analysis for the different categories, as well as their final contamination to the candidate sample after correcting for trigger efficiency, lepton ID and N_{jet} scale factor.

For the $W\gamma$ background, given that the second lepton comes from photon conversion misidentification, we applied a conversion inefficiency scale factor equal SF_{conv} = 1.2 ± 0.12, according to the study reported in CDF-8073. The final correction factor has to be convoluted with the numbers of electrons from photon with E_T < 40 GeV and found equal to 1.147 for $W\gamma \to e\nu\gamma$ events and 1.161 for $W\gamma \to \mu\nu\gamma$ events.

The systematic uncertainties on these backgrounds come from different sources as discussed in detail in section 6.

5.3 Drell-Yan background

The background from DY/$Z \to ee$ and $\mu\mu$ is based on the number of data events observed in the Z region with high missing transverse energy, after correcting for the presence of non DY/Z events. This remaining DY/Z contamination to the candidate region is calculated as two separate contributions: events outside the Z-peak region(N_{OUT}) and events inside the Z-peak region passing the Z-veto (N_{IN}). We calculated N_{IN} and N_{OUT} from separate data estimates in the 0-jet, 1-jet and 2-jet data bins. We still use the DY/$Z \to ee$ and DY/$Z \to \mu\mu$ Monte Carlo to predict the ratio of events in different kinematic regions, as explained below.

The background for each j-th jet multiplicity bin is extracted from the following equations:

$$\begin{aligned} N^j_{DY} &= N^j_{OUT} + N^j_{IN} \\ N^j_{OUT} &= R^{out/in,\,j}_{\not{E}_T}(N^{DT,\,j}_{\not{E}_T} - N^{BKG,\,j}_{\not{E}_T}) \\ N^j_{IN} &= R^{high/low,\,j}_{Zveto}(N^{DT,\,j}_{Zveto} - N^{BKG,\,j}_{Zveto}) \end{aligned} \quad (4)$$

where the subscript "$\not{E}_T$" refers to dilepton events in the 76-106 GeV invariant mass region after the $\not{E}_T$ and L-cut but before the Z-veto cut; and the subscript "Zveto" refers to the subsample of these same events failing the Z-veto cut (i.e. with MetSig $< 4\ \sqrt{\mathrm{GeV}}$). $N^{DT,\,j}$ is the number of events observed in data in each jet bin and $N^{BKG,\,j}$ is the non-DY background coming from the $Z \to \tau\tau$, top, diboson and fake lepton sources. $R^{out/in}$ is the ratio of events with dilepton invariant mass outside over inside the 76-106 GeV peak region. Finally $R^{high/low}$ is the Monte Carlo ratio of events within the Z peak region with high over low Met significance. These ratios are measured using Alpgen all DY/Z MC events per each jet multiplicity bin. Tables 8 and 9 summarize the value of each term used to calculate the the N^j_{OUT} and N^j_{IN} fake contributions in equations 4.

Input	After $\not{E}_T$ and L-cut					
	0-jet		1-jet		≥2-jet	
	ee	$\mu\mu$	ee	$\mu\mu$	ee	$\mu\mu$
$N^{DT}_{\not{E}_T}$	363	247	397	245	323	200
$N^{BKG}_{\not{E}_T}$	83.3±3.9	62.9±3.7	55.9±4.8	39.4±4.8	60.6±3.9	51.4±3.2
$R^{out/in}$	0.33±0.05	0.23±0.07	0.24±0.04	0.17±0.04	0.18±0.02	0.19±0.02
N_{OUT}	90.34±7.85	31.97±4.05	80.57±5.70	34.46±3.08	48.27±3.47	28.39±2.84

Table 8: Inputs to equation 4 used to calculate N^j_{OUT}, the DY/$Z \to ee$ and $\mu\mu$ background contamination outside the Z peak region. The last row is the final N^j_{OUT} for each dilepton flavour and jet multiplicity.

Input	After $\not\!\!E_T$, L-cut and Z-veto					
	0-jet		1-jet		≥2-jet	
	ee	$\mu\mu$	ee	$\mu\mu$	ee	$\mu\mu$
N^{DT}_{Zveto}	329	177	376	234	301	183
N^{BKG}_{Zveto}	34.2±1.7	31.3±2.8	16.5±1.6	14.3±1.4	19.9±0.5	21.6 ±1.3
$R^{high/low}$	0.0028±0.0012	0.0004±0.0002	0.0096±0.0021	0.0072±0.0024	0.0112±0.0010	0.0102±0.0015
N_{IN}	0.76±0.05	0.06±0.01	3.23±0.19	1.51±0.11	2.91±0.19	1.57±0.14

Table 9: Inputs to equation 4 used to calculate N^j_{IN}, the DY/$Z \rightarrow ee$ and $\mu\mu$ background contamination inside the Z peak region. The last row is the final N^j_{IN} for each dilepton flavour and jet multiplicity.

ϵ_{HT}	ee	$\mu\mu$
After $\not\!\!E_T$ and L-cut	0.40±0.03	0.55±0.04
After $\not\!\!E_T$, L-cut and Z-veto	0.93±0.02	0.98±0.03

Table 10: H_T and opposite sign cut efficiency for the DY/$Z \rightarrow ee$ and $\mu\mu$ background contamination in ≥ 2 jet region. The efficiency is calculated separately for the outside Z peak region, after applying only the $\not\!\!E_T$ and L-cut, and the inside Z peak region, after applying also the Z-veto.

The DY/Z contamination to the final top DIL candidate region is extracted from the N^2_{OUT} and N^2_{IN} estimates in the ≥ 2 jet bin after multiplying by the efficiency of the H_T plus opposite sign cut, ϵ_{HT}. The ϵ_{HT} efficiencies, shown in Table 10, are calculated using the Alpgen all Z samples.

We also estimate the contamination of DY/$Z \rightarrow \mu\mu$ events to the $e\mu$ category. Monte Carlo studies have shown that this contamination comes from events where one of the final state muon events had a very energetic photon from final state radiation. The photon, almost collinear to the muon, deposits its energy in the EM calorimeter. This EM cluster is then associated to the original muon track to fake the electron signature. As no data based control sample is available for this contamination, we estimate it using the Monte Carlo prediction. And when we substract expected top quark events in DY/Z sample, we used the Standard Model prediction of 7.4 pb for the $t\bar{t}$ cross section for $M_{top} = 172.5$ GeV.

5.4 Fake Lepton background

Jets with large energy deposit in the electromagnetic calorimeter and a single high p_T track can fake electrons. They can fake a muon if their hadron activity produce single pions or kaons with a later shower. Heavy flavor production can also result in real high p_T lepton from semileptonic b and c hadron decays.

These jets faking a lepton can produce a final state with two leptons and possibly other jets when they accompany the lepton plus $\not\!\!E_T$ signature generated by W+jets events. We measure the fake lepton background by weighting fakeable jets in W+jets events with a fake rate probability estimated from the QCD data.

The fake rate is a lepton type dependent probability that a fakeable object, that is an object which shares some of the jets and some of the high p_T lepton characteristics, can be reconstructed as a good lepton. A fakeable object is narrowly defined as a CDF_EM object with HAD/EM energy deposition < 0.125 or a CDF Muons with E/p< 1. To remove real lepton contamination in W+jet events from Z and Diboson, fakeable object is required to have at least one failure of the ID cut, shown in Table 11, as a anti-cut. In order to increase the statistics of fakeable objects we allow both stub and stubless muons i.e. we have CMUP fiducial CMUP stubbless muon in fakeable object.

	List of anti-cut variables
TCEM, NCEM	HAD/EM, Strip Chi2, LShr, CEM DEltaX, CES DeltaZ
TPHX	HAD/EM, Pem3x3FitTow, Pem3x3Chi2, preProfileratio5by9U, preProfileratio5by9V
TCMUP, TCMUX, LMUO, NMUO	Stubb, HAD, EM, stub deltaX
LMIO	HAD, EM, total E, stub deltaX(only CMX minikey)

Table 11: Anti-cut variables. Fakeable events require at least one of these ID cuts.

The reconstructed fake leptons can be include with real leptons from W, DY, and Diboson. So it is necessary to remove the real lepton contamination in the QCD jet sample. The MC samples for (DY$\rightarrow$ ee(zewkad), DY$\rightarrow$ $\mu\mu$(zewk9m), DY$\rightarrow$ $\tau\tau$(zewkat), WW(itopww), WZ(itopwz), ZZ(itopzz))is used to estimate this real lepton contamination. Jet threshold E_T is increased as corresponding to 90% trigger efficiency for the comparison with the MC events. it is possible to mimic the trigger turn on curve by using E_T of 35, 55, 75 and 105 GeV corresponding to the jet20, jet50, jet70 and jet 100 triggers.

Real lepton is calculated using the following equation:

$$\text{RealLepton}_{MC} = \frac{\text{Acc}_{MC} \times \sigma_{MC} \times \text{lum}_{jet}}{\text{EffectivePS}_{jet}} \tag{5}$$

"Acc" is each MC's one lepton and more than one threshold E_T jet acceptance. "lum" is luminosity of each QCD jet sample. "Effective PS$_{jet}$" is sum of each run's weighted pre-scale by each run's luminosity. QCD jet sample's detail parameter is Table 12 We subtract this real lepton contamination from jet sample's good lepton and fakeable object. Fake Rate is calculated using the following equation:

$$\text{FakeRate} = \frac{\text{GoodLepton}_{jet} - \text{RealLepton}_{MC}}{\text{Fakeable}_{jet} - \text{RealFakeable}_{MC}} \tag{6}$$

Where the subscript "jet" refers to number estimated from the QCD jet sample; and the subscript "MC" refers to number from the MC prediction. "GoodLepton" is number of reconstructed lepton in QCD jet sample. "RealLepton" is the number of fakeable in QCD jet sample. "RealLepton" and "RealFakeable" are number of good lepton and fakeable predicted by MC, i.e. the real lepton contamination.

	jet20	jet50	jet70	jet100
luminosity	9027.12 pb^{-1}	9028.68 pb^{-1}	9028.11 pb^{-1}	9028.76 pb^{-1}
Effective pre-scale	2341.02	81.02	8	1
jet E_T threshold cut	35 GeV	55 GeV	75 GeV	105 GeV

Table 12: Some parameter of QCD jet sample, and jet E_T threshold cut value to ensure 90% trigger efficiency.

Depending on the geometrical region where the fakeable points to, we define separate fakeable categories for CEM and PHX electrons (TCEM and TPHX), and for CMUP, CMX, CMU/CMP and CMIO muons (TMUO, TCMX, LMUO and LMIO). For non isolated leptons (NCEM and NMUO), we require that the fakeable object is also non isolated.

Using the JET50 QCD data sample, we calculated the fake rates reported in Table 14, **??** and shown in Figure 15. The six variable-width p_T bins ([20–30] GeV, [30–40] GeV, [40–60] GeV, [60–100] GeV,[100–200] GeV and $\geq$ 200 GeV) are chosen so to have a reasonable statistics in each bin.

Figure 16 shows a comparison between the number of fake lepton events observed in the JET20, JET70 and JET100 data sample, integrated over the full p_T spectrum, and what is predicted by the JET50 fake rate matrix. Based on this plot, we assess a 30% systematic uncertainty for the JET50-based electron and muon fake rate estimate.

The fake lepton contamination to the control bins and to the top DIL candidate sample are calculated by weighting each "lepton+fakeable" event by the appropriate fake rate in Table 14, **??** and summing all of the fake contributions together. We define as "lepton+fakeable" any event in the central high p_T lepton datasets with one and only one good high pT lepton, $\not\!\!E_T$ >25 GeV and a second fakeable object, and passing the anti-cut. The fakeable object, which can be from any of the fake categories defined above, is paired to the good lepton and treated as the second lepton in the event when calculating any of the kinematic variables used in the top DIL selection (dilepton invariant mass, corrected $\not\!\!E_T$, H_T..). Tight jets found in a cone of $\Delta R < 0.4$ around the fakeable lepton are dropped from the tight jet counting of that event. The fakeable object is allowed to be the trigger lepton if it belongs to TCEM, TCMUP or TCMX category. If more than one fakeable object is found in the event, we pair each of them to the good lepton.

The fake lepton uncertainty contains a statistical component, which is the sum of the fake rate uncertainty itself and the statistics of the "lepton+fakeable" sample, and a systematic component coming from the 30% fake rate systematic uncertainty derived from Figure 16. When summing together the fake rate from different "lepton+fakeable" dilepton categories, the 30% uncertainties in fake ee and in fake $\mu\mu$ pairs (i.e. good electron plus fakeable electron and good muon plus fakeable muon pairs) are assumed to be uncorrelated and summed in quadrature while the 30% uncertainty of fake $e\mu$ pairs (i.e. good electron paired to a fakeable muon or good muon paired to a fakeable electron) is considered fully correlated and added linearly.

We compare our same sign fake background estimation and same sign dilepton candidate in the signal region. We are using fakeable lepton's charge as fake lepton's charge. Same sign dilepton candidate after subtraction of standard model same sign events are fake lepton. Therefore comparison of our same sign fake background and data's same sign candidate is good check of our fake background estimation method. Check results are given in Table 13. We remove Drell-Yan and Diboson MC's same sign events from data same sign dilepton candidate as standard model same sign events. Results is very consistent.

	ee	$\mu\mu$	$e\mu$	all
SS in the data of 0-jet	27.52 ± 7.94	51.18 ± 7.42	52.81 ± 9.70	131.52 ± 14.56
Measured SS fake in 0-jet	21.31 ± 6.52	35.79 ± 11.49	57.64 ± 17.74	114.75 ± 26.57
SS in the data of 1-jet	14.47 ± 5.66	22.42 ± 4.90	81.78 ± 10.10	118.67 ± 12.57
Measured SS fake in 1-jet	15.86 ± 4.85	23.54 ± 7.52	75.50 ± 23.06	114.89 ± 17.80
SS in the data of jets (≥ 2)	17.20 ± 5.39	9.84 ± 3.46	69.43 ± 9.06	96.47 ± 11.09
Measured SS fake in jets (≥ 2)	12.82 ± 3.95	25.32 ± 7.96	78.17 ± 23.85	116.31 ± 19.01

Table 13: Comparison between our same sing fake background and data same sign dilepton candidate after subtraction of standard model same sign events.

Fake lepton	JET50 Fake rate for period 0 ∼ 8					
	[20–30] GeV	[30–40] GeV	[40–60] GeV	[60–100] GeV	[100–200] GeV	$p_T \geq 200$ GeV
TCEM	0.0490 ± 0.0014	0.0390 ± 0.0011	0.0237 ± 0.0002	0.0274 ± 0.0003	0.0356 ± 0.0016	0.0632 ± 0.0509
NCEM	0.0077 ± 0.0000	0.0053 ± 0.0000	0.0058 ± 0.0000	0.0051 ± 0.0001	0.0046 ± 0.0011	0.0000 ± 0.0000
TPHX	0.1363 ± 0.0013	0.1306 ± 0.0017	0.1213 ± 0.0002	0.1970 ± 0.0003	0.2671 ± 0.0034	0.4830 ± 0.7842
TCMUP	0.0122 ± 0.0007	0.0293 ± 0.0019	0.0411 ± 0.0027	0.0832 ± 0.0056	0.0638 ± 0.0135	0.0000 ± 0.0000
TCMX	0.0105 ± 0.0011	0.0229 ± 0.0032	0.0533 ± 0.0049	0.0960 ± 0.0147	0.0055 ± 0.2238	0.0000 ± 0.0000
LMUO	0.0320 ± 0.0008	0.0426 ± 0.0024	0.0554 ± 0.0046	0.0805 ± 0.0108	0.1461 ± 0.0191	0.0100 ± 0.0059
LMIO	0.1977 ± 0.0013	0.2139 ± 0.0043	0.2110 ± 0.0060	0.3414 ± 0.0140	0.1921 ± 0.0289	0.9250 ± 0.0288
NMUO	0.0053 ± 0.0000	0.0037 ± 0.0000	0.0022 ± 0.0000	0.0020 ± 0.0001	0.0012 ± 0.0007	0.0034 ± 0.0034

Fake lepton	JET50 Fake rate for period 9 ∼ 12					
	[20–30] GeV	[30–40] GeV	[40–60] GeV	[60–100] GeV	[100–200] GeV	$p_T \geq 200$ GeV
TCEM	0.0392 ± 0.0060	0.0198 ± 0.0067	0.0246 ± 0.0005	0.0327 ± 0.0009	0.0232 ± 0.0067	0.0642 ± 0.1390
NCEM	0.0072 ± 0.0000	0.0048 ± 0.0000	0.0055 ± 0.0000	0.0045 ± 0.0002	0.0221 ± 0.0033	0.0000 ± 0.0000
TPHX	0.1280 ± 0.0046	0.1860 ± 0.0063	0.1256 ± 0.0007	0.2195 ± 0.0009	0.2478 ± 0.0113	0.0000 ± 0.0000
TCMUP	0.0084 ± 0.0019	0.0200 ± 0.0044	0.0426 ± 0.0049	0.0660 ± 0.0093	0.0442 ± 0.0127	0.0000 ± 0.0000
TCMX	0.0079 ± 0.0023	0.0288 ± 0.0054	0.0326 ± 0.0070	0.0380 ± 0.0156	0.0023 ± 0.0755	0.0074 ± 0.0079
LMUO	0.0150 ± 0.0022	0.0158 ± 0.0066	0.0318 ± 0.0079	0.0065 ± 0.0604	0.0241 ± 0.0232	0.0000 ± 0.0000
LMIO	0.1949 ± 0.0045	0.2754 ± 0.0120	0.4840 ± 0.0212	0.4879 ± 0.0308	0.4417 ± 0.0463	1.1712 ± 0.0621
NMUO	0.0046 ± 0.0000	0.0036 ± 0.0000	0.0023 ± 0.0001	0.0036 ± 0.0002	0.0063 ± 0.0016	0.0000 ± 0.0000

Fake lepton	JET50 Fake rate for period 13 ∼ 17					
	[20–30] GeV	[30–40] GeV	[40–60] GeV	[60–100] GeV	[100–200] GeV	$p_T \geq 200$ GeV
TCEM	0.0637 ± 0.0050	0.0479 ± 0.0050	0.0243 ± 0.0007	0.0301 ± 0.0011	0.0320 ± 0.0068	0.0000 ± 0.0000
NCEM	0.0065 ± 0.0000	0.0057 ± 0.0000	0.0060 ± 0.0000	0.0044 ± 0.0002	0.0039 ± 0.0047	0.0000 ± 0.0000
TPHX	0.0823 ± 0.0058	0.1186 ± 0.0076	0.1523 ± 0.0009	0.2163 ± 0.0011	0.3018 ± 0.0155	0.0000 ± 0.0000
TCMUP	0.0045 ± 0.0028	0.0103 ± 0.0059	0.0258 ± 0.0067	0.0198 ± 0.0168	0.0129 ± 0.0180	0.0000 ± 0.0000
TCMX	0.0072 ± 0.0025	0.0132 ± 0.0065	0.0535 ± 0.0069	0.0117 ± 0.0280	0.0149 ± 0.0216	0.0078 ± 0.0082
LMUO	0.0148 ± 0.0028	0.0089 ± 0.0085	0.0330 ± 0.0113	0.0608 ± 0.0122	0.0519 ± 0.0178	0.0000 ± 0.0000
LMIO	0.2775 ± 0.0057	0.3499 ± 0.0137	0.2828 ± 0.0209	0.4562 ± 0.0363	0.8478 ± 0.1307	1.2367 ± 0.0589
NMUO	0.0046 ± 0.0000	0.0032 ± 0.0001	0.0025 ± 0.0001	0.0034 ± 0.0003	0.0040 ± 0.0021	0.0000 ± 0.0000

Fake lepton	JET50 Fake rate for period 18 ∼ 19					
	[20–30] GeV	[30–40] GeV	[40–60] GeV	[60–100] GeV	[100–200] GeV	$p_T \geq 200$ GeV
TCEM	0.0693 ± 0.0064	0.0322 ± 0.0080	0.0258 ± 0.0009	0.0263 ± 0.0015	0.0680 ± 0.0065	0.0000 ± 0.0000
NCEM	0.0066 ± 0.0000	0.0054 ± 0.0001	0.0063 ± 0.0001	0.0038 ± 0.0003	0.0109 ± 0.0059	0.0000 ± 0.0000
TPHX	0.1625 ± 0.0144	0.1362 ± 0.0122	0.1244 ± 0.0013	0.2021 ± 0.0017	0.2219 ± 0.0231	0.0000 ± 0.0000
TCMUP	0.0141 ± 0.0025	0.0183 ± 0.0059	0.0190 ± 0.0111	0.0962 ± 0.0135	0.0217 ± 0.0210	0.0000 ± 0.0000
TCMX	0.0032 ± 0.0050	0.0136 ± 0.0091	0.0585 ± 0.0102	0.0263 ± 0.0327	0.0260 ± 0.0291	0.0000 ± 0.0000
LMUO	0.0061 ± 0.0047	0.0131 ± 0.0097	0.0281 ± 0.0144	0.0857 ± 0.0171	0.0071 ± 0.0792	0.0000 ± 0.0000
LMIO	0.2718 ± 0.0064	0.4669 ± 0.0229	0.4642 ± 0.0283	0.9887 ± 0.0789	0.5727 ± 0.0682	1.2271 ± 0.1013
NMUO	0.0052 ± 0.0000	0.0035 ± 0.0001	0.0037 ± 0.0001	0.0034 ± 0.0004	0.0055 ± 0.0029	0.0000 ± 0.0000

Fake lepton	JET50 Fake rate for period 20 ∼ 23					
	[20–30] GeV	[30–40] GeV	[40–60] GeV	[60–100] GeV	[100–200] GeV	$p_T \geq 200$ GeV
TCEM	0.0591 ± 0.0039	0.0468 ± 0.0033	0.0252 ± 0.0005	0.0326 ± 0.0008	0.0251 ± 0.0052	0.1146 ± 0.0965
NCEM	0.0072 ± 0.0000	0.0055 ± 0.0000	0.0061 ± 0.0000	0.0061 ± 0.0001	0.0046 ± 0.0027	0.0000 ± 0.0000
TPHX	0.1043 ± 0.0045	0.1358 ± 0.0051	0.1528 ± 0.0006	0.2299 ± 0.0008	0.2153 ± 0.0091	0.0000 ± 0.0000
TCMUP	0.0045 ± 0.0021	0.0053 ± 0.0054	0.0227 ± 0.0044	0.0230 ± 0.0094	0.0116 ± 0.0143	0.0000 ± 0.0000
TCMX	0.0034 ± 0.0025	0.0100 ± 0.0044	0.0249 ± 0.0062	0.0077 ± 0.0273	0.0078 ± 0.0207	0.0047 ± 0.0051
LMUO	0.0138 ± 0.0019	0.0245 ± 0.0039	0.0334 ± 0.0058	0.0319 ± 0.0118	0.0320 ± 0.0138	0.0000 ± 0.0000
LMIO	0.3252 ± 0.0042	0.4322 ± 0.0113	0.4723 ± 0.0151	0.7978 ± 0.0374	0.9172 ± 0.0482	0.9823 ± 0.0348
NMUO	0.0050 ± 0.0000	0.0031 ± 0.0000	0.0031 ± 0.0000	0.0018 ± 0.0002	0.0025 ± 0.0014	0.0063 ± 0.0064

Fake lepton	JET50 Fake rate for period 24 ∼ 25					
	[20–30] GeV	[30–40] GeV	[40–60] GeV	[60–100] GeV	[100–200] GeV	$p_T \geq 200$ GeV
TCEM	0.0765 ± 0.0074	0.0377 ± 0.0079	0.0337 ± 0.0010	0.0162 ± 0.0026	0.0458 ± 0.0080	0.4421 ± 0.8627
NCEM	0.0068 ± 0.0000	0.0059 ± 0.0001	0.0059 ± 0.0001	0.0053 ± 0.0003	0.0050 ± 0.0056	0.0000 ± 0.0000
TPHX	0.1234 ± 0.0119	0.1336 ± 0.0117	0.1381 ± 0.0014	0.2176 ± 0.0019	0.3784 ± 0.0266	0.0000 ± 0.0000
TCMUP	0.0037 ± 0.0039	0.0047 ± 0.0137	0.0064 ± 0.0211	0.0219 ± 0.0164	0.0348 ± 0.0163	0.0000 ± 0.0000
TCMX	0.0134 ± 0.0038	0.0366 ± 0.0082	0.0004 ± 0.2609	0.0890 ± 0.0174	0.0093 ± 0.0359	0.0000 ± 0.0000
LMUO	0.0141 ± 0.0042	0.0172 ± 0.0107	0.0078 ± 0.0337	0.0416 ± 0.0246	0.0188 ± 0.0210	0.0000 ± 0.0000
LMIO	0.2387 ± 0.0092	0.4677 ± 0.0297	0.4688 ± 0.0355	0.5398 ± 0.0470	0.7550 ± 0.1414	1.0344 ± 0.0702
NMUO	0.0042 ± 0.0000	0.0034 ± 0.0001	0.0023 ± 0.0001	0.0023 ± 0.0005	0.0030 ± 0.0032	0.0000 ± 0.0000

Fake lepton	JET50 Fake rate for period 26 ∼ 28					
	[20–30] GeV	[30–40] GeV	[40–60] GeV	[60–100] GeV	[100–200] GeV	$p_T \geq 200$ GeV
TCEM	0.0488 ± 0.0069	0.0336 ± 0.0053	0.0348 ± 0.0006	0.0293 ± 0.0011	0.0041 ± 0.0281	0.0000 ± 0.0000
NCEM	0.0066 ± 0.0000	0.0055 ± 0.0000	0.0061 ± 0.0000	0.0043 ± 0.0002	0.0068 ± 0.0038	0.0000 ± 0.0000
TPHX	0.1065 ± 0.0053	0.1081 ± 0.0072	0.1337 ± 0.0008	0.2381 ± 0.0010	0.2754 ± 0.0146	0.0000 ± 0.0000
TCMUP	0.0044 ± 0.0029	0.0128 ± 0.0053	0.0116 ± 0.0123	0.0320 ± 0.0116	0.0131 ± 0.0200	0.0000 ± 0.0000
TCMX	0.0074 ± 0.0027	0.0172 ± 0.0060	0.0330 ± 0.0080	0.0637 ± 0.0124	0.0302 ± 0.0210	0.0174 ± 0.0091
LMUO	0.0174 ± 0.0024	0.0182 ± 0.0070	0.0588 ± 0.0085	0.0693 ± 0.0147	0.0292 ± 0.0246	0.0000 ± 0.0000
LMIO	0.2936 ± 0.0057	0.2715 ± 0.0153	0.3988 ± 0.0173	0.4876 ± 0.0400	1.0831 ± 0.1030	0.5832 ± 0.0330
NMUO	0.0049 ± 0.0000	0.0043 ± 0.0000	0.0022 ± 0.0001	0.0037 ± 0.0003	0.0000 ± 0.0000	0.0078 ± 0.0079

Fake lepton	JET50 Fake rate for period 29 ∼ 31					
	[20–30] GeV	[30–40] GeV	[40–60] GeV	[60–100] GeV	[100–200] GeV	$p_T \geq 200$ GeV
TCEM	0.1041 ± 0.0043	0.0300 ± 0.0050	0.0319 ± 0.0005	0.0226 ± 0.0011	0.0412 ± 0.0050	0.0594 ± 0.1274
NCEM	0.0073 ± 0.0000	0.0058 ± 0.0000	0.0058 ± 0.0000	0.0039 ± 0.0002	0.0000 ± 0.0000	0.0000 ± 0.0000
TPHX	0.1461 ± 0.0055	0.1175 ± 0.0071	0.1288 ± 0.0007	0.2060 ± 0.0011	0.2597 ± 0.0112	0.0000 ± 0.0000
TCMUP	0.0011 ± 0.0054	0.0165 ± 0.0036	0.0043 ± 0.0148	0.0346 ± 0.0070	0.0296 ± 0.0067	0.0000 ± 0.0000
TCMX	0.0029 ± 0.0031	0.0125 ± 0.0047	0.0202 ± 0.0067	0.0618 ± 0.0086	0.0480 ± 0.0099	0.0000 ± 0.0000
LMUO	0.0097 ± 0.0024	0.0188 ± 0.0057	0.0437 ± 0.0066	0.0572 ± 0.0085	0.0296 ± 0.0110	0.0000 ± 0.0000
LMIO	0.3088 ± 0.0048	0.4788 ± 0.0115	0.5536 ± 0.0180	0.7117 ± 0.0343	0.7344 ± 0.0458	1.2380 ± 0.0533
NMUO	0.0047 ± 0.0000	0.0042 ± 0.0000	0.0024 ± 0.0001	0.0031 ± 0.0003	0.0016 ± 0.0018	0.0129 ± 0.0065

Fake lepton	JET50 Fake rate for period 32 ∼ 34					
	[20–30] GeV	[30–40] GeV	[40–60] GeV	[60–100] GeV	[100–200] GeV	$p_T \geq 200$ GeV
TCEM	0.0475 ± 0.0058	0.0554 ± 0.0037	0.0299 ± 0.0005	0.0367 ± 0.0008	0.0452 ± 0.0047	0.0000 ± 0.0000
NCEM	0.0069 ± 0.0000	0.0057 ± 0.0000	0.0067 ± 0.0000	0.0064 ± 0.0002	0.0076 ± 0.0028	0.0000 ± 0.0000
TPHX	0.1537 ± 0.0054	0.0983 ± 0.0074	0.1412 ± 0.0007	0.2239 ± 0.0009	0.3459 ± 0.0113	0.0000 ± 0.0000
TCMUP	0.0025 ± 0.0029	0.0035 ± 0.0077	0.0177 ± 0.0047	0.0265 ± 0.0070	0.0009 ± 0.0798	0.0000 ± 0.0000
TCMX	0.0109 ± 0.0016	0.0189 ± 0.0038	0.0131 ± 0.0075	0.0297 ± 0.0075	0.0117 ± 0.0108	0.0091 ± 0.0047
LMUO	0.0130 ± 0.0021	0.0107 ± 0.0052	0.0044 ± 0.0167	0.0401 ± 0.0095	0.0244 ± 0.0103	0.0083 ± 0.0044
LMIO	0.3437 ± 0.0042	0.4289 ± 0.0101	0.4593 ± 0.0128	0.6887 ± 0.0210	1.1706 ± 0.0493	0.9999 ± 0.0308
NMUO	0.0039 ± 0.0000	0.0036 ± 0.0000	0.0025 ± 0.0001	0.0016 ± 0.0002	0.0028 ± 0.0015	0.0000 ± 0.0000

Fake lepton	JET50 Fake rate for period 35 ∼ 38					
	[20–30] GeV	[30–40] GeV	[40–60] GeV	[60–100] GeV	[100–200] GeV	$p_T \geq 200$ GeV
TCEM	0.0524 ± 0.0048	0.0551 ± 0.0035	0.0228 ± 0.0005	0.0255 ± 0.0009	0.0274 ± 0.0055	0.0516 ± 0.1306
NCEM	0.0073 ± 0.0000	0.0059 ± 0.0000	0.0061 ± 0.0000	0.0052 ± 0.0002	0.0025 ± 0.0032	0.0000 ± 0.0000
TPHX	0.1131 ± 0.0052	0.1203 ± 0.0075	0.1422 ± 0.0007	0.1996 ± 0.0009	0.2841 ± 0.0114	0.0000 ± 0.0000
TCMUP	0.0093 ± 0.0015	0.0053 ± 0.0053	0.0155 ± 0.0041	0.0269 ± 0.0052	0.0116 ± 0.0077	0.0000 ± 0.0000
TCMX	0.0069 ± 0.0018	0.0167 ± 0.0034	0.0178 ± 0.0055	0.0315 ± 0.0057	0.0104 ± 0.0096	0.0000 ± 0.0000
LMUO	0.0092 ± 0.0021	0.0149 ± 0.0040	0.0252 ± 0.0050	0.0232 ± 0.0083	0.0377 ± 0.0076	0.0037 ± 0.0041
LMIO	0.3693 ± 0.0047	0.4685 ± 0.0109	0.4567 ± 0.0112	0.9034 ± 0.0256	0.8916 ± 0.0327	0.9332 ± 0.0258
NMUO	0.0046 ± 0.0000	0.0033 ± 0.0000	0.0024 ± 0.0000	0.0029 ± 0.0002	0.0000 ± 0.0000	0.0000 ± 0.0000

Table 14: JET50 fake rates vs lepton p_T range for different fakeable objects for later dataset period.

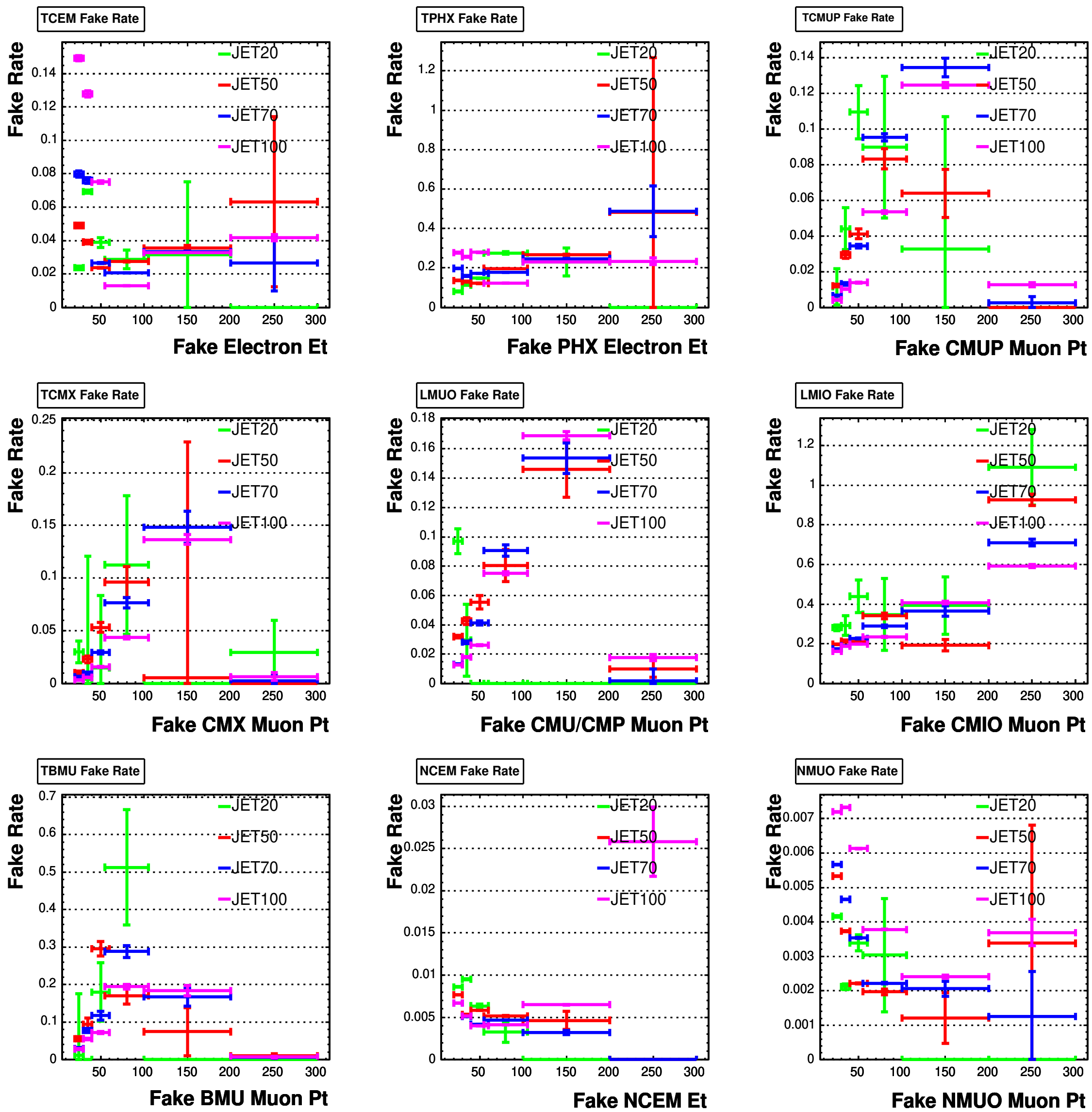

Figure 6: Fake rate estimates versus lepton p_T for each fakeable category in the date period $0 \sim 8$. The JET50 fake rates, shown in red, are compared to the JET20 (green), JET70 (blue) and JET100 (magenta) fake rates. TBMU fakeable objects are not used in this analysis.

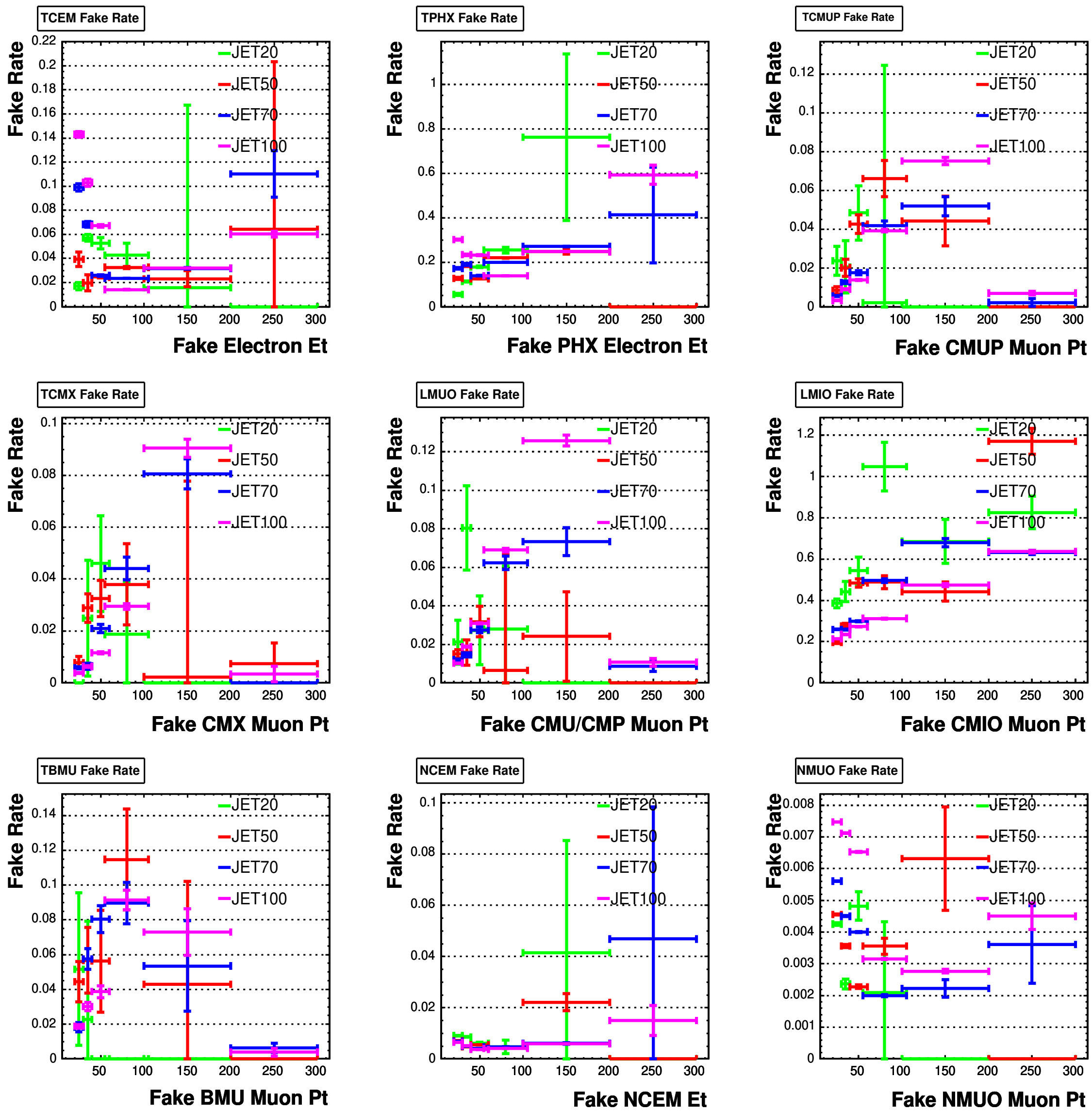

Figure 7: Fake rate estimates versus lepton p_T for each fakeable category in the date period $9 \sim 12$. The JET50 fake rates, shown in red, are compared to the JET20 (green), JET70 (blue) and JET100 (magenta) fake rates. TBMU fakeable objects are not used in this analysis.

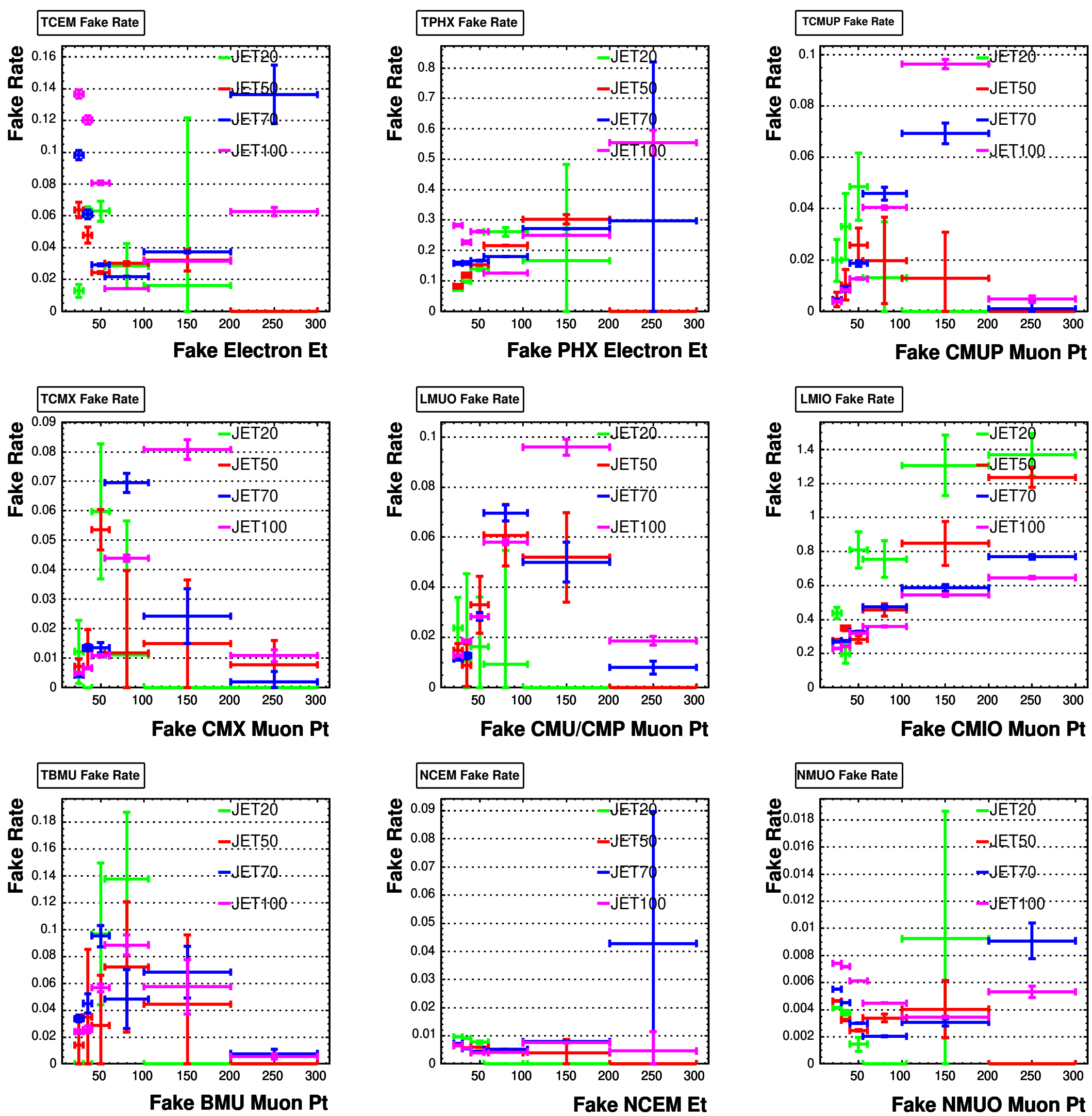

Figure 8: Fake rate estimates versus lepton p_T for each fakeable category in the date period 13 $\sim$ 17. The JET50 fake rates, shown in red, are compared to the JET20 (green), JET70 (blue) and JET100 (magenta) fake rates. TBMU fakeable objects are not used in this analysis.

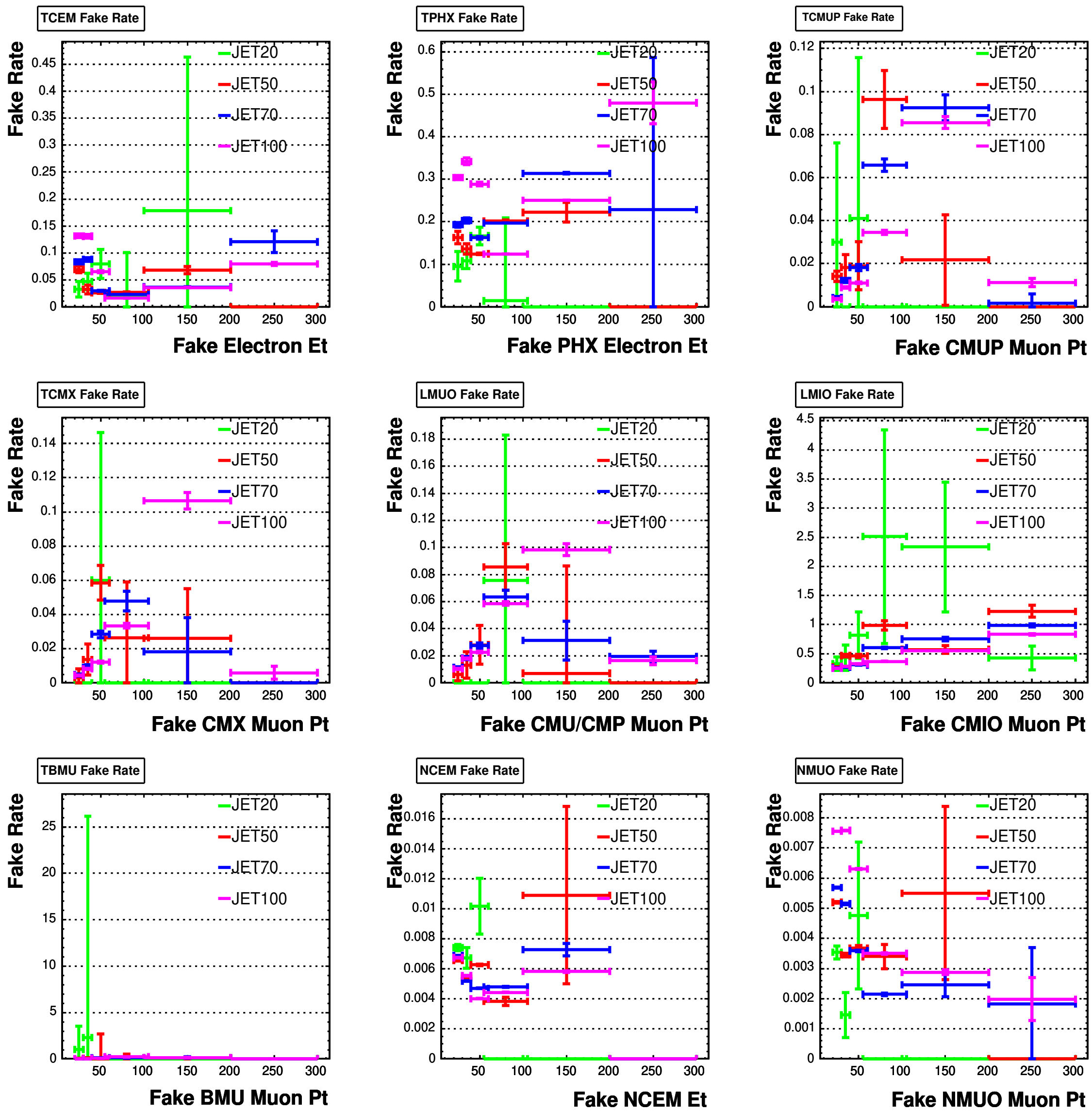

Figure 9: Fake rate estimates versus lepton p_T for each fakeable category in the date period 18 $\sim$ 19. The JET50 fake rates, shown in red, are compared to the JET20 (green), JET70 (blue) and JET100 (magenta) fake rates. TBMU fakeable objects are not used in this analysis.

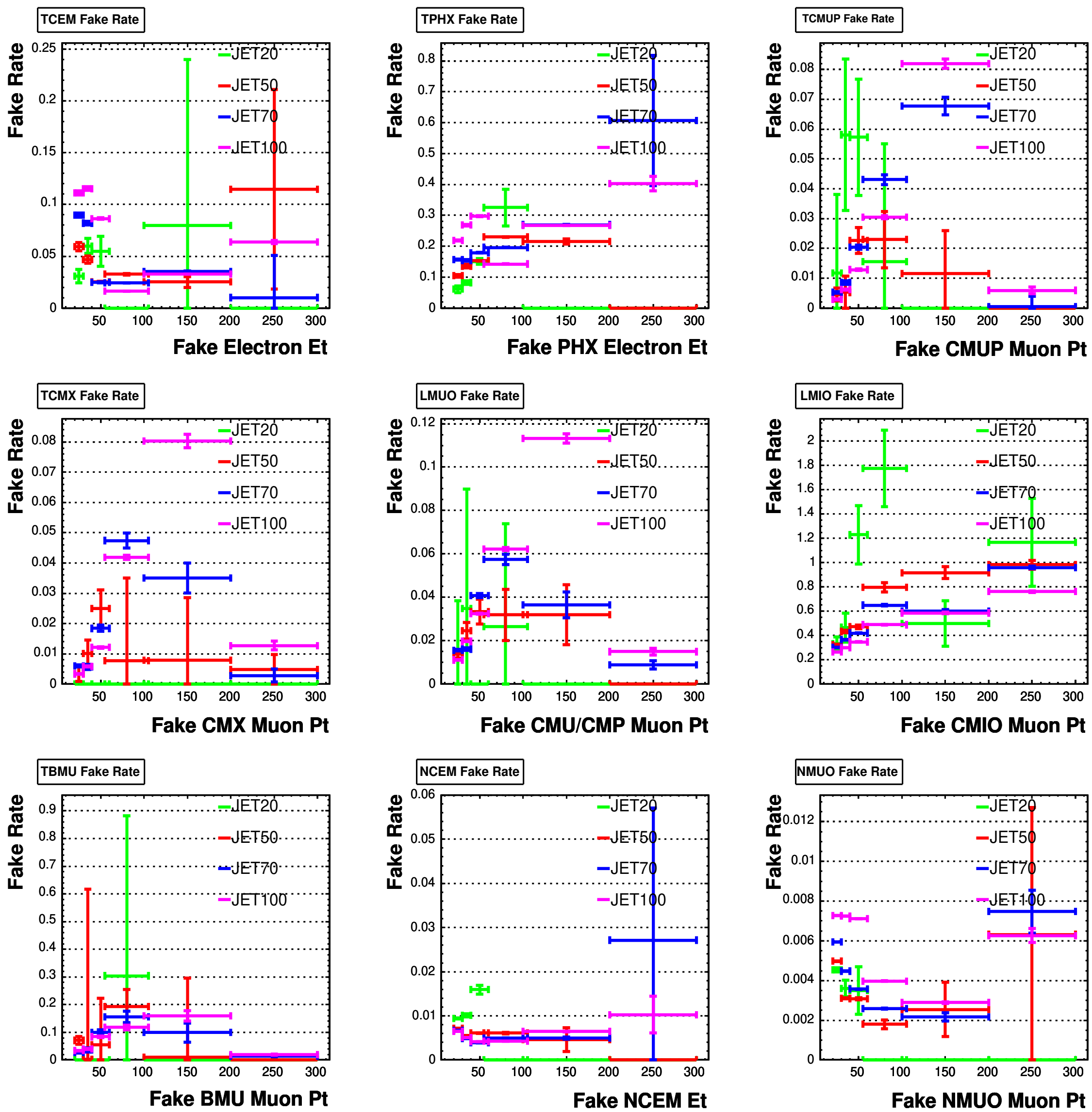

Figure 10: Fake rate estimates versus lepton p_T for each fakeable category in the date period 20 $\sim$ 23. The JET50 fake rates, shown in red, are compared to the JET20 (green), JET70 (blue) and JET100 (magenta) fake rates. TBMU fakeable objects are not used in this analysis.

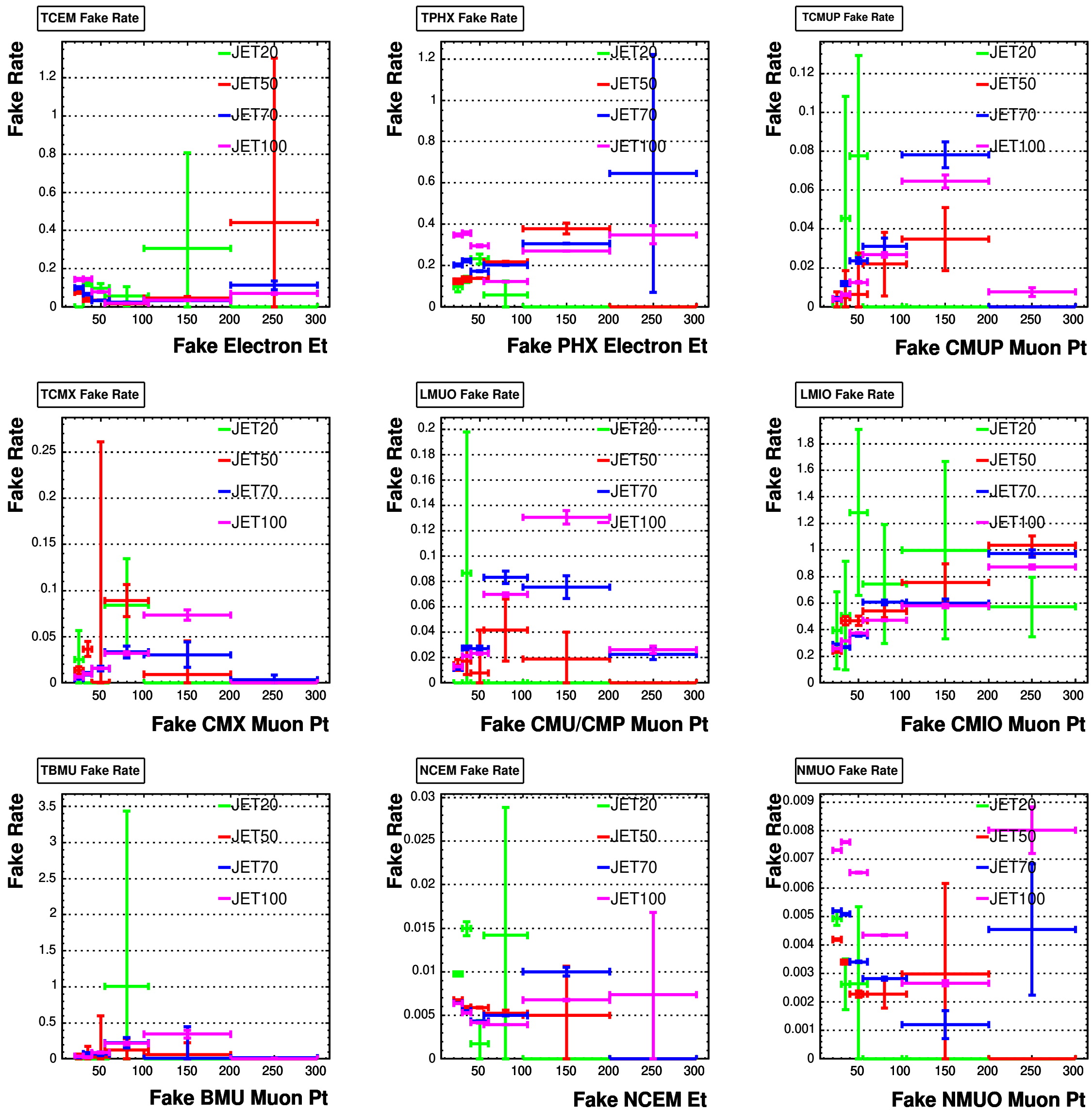

Figure 11: Fake rate estimates versus lepton p_T for each fakeable category in the date period 24 $\sim$ 25. The JET50 fake rates, shown in red, are compared to the JET20 (green), JET70 (blue) and JET100 (magenta) fake rates. TBMU fakeable objects are not used in this analysis.

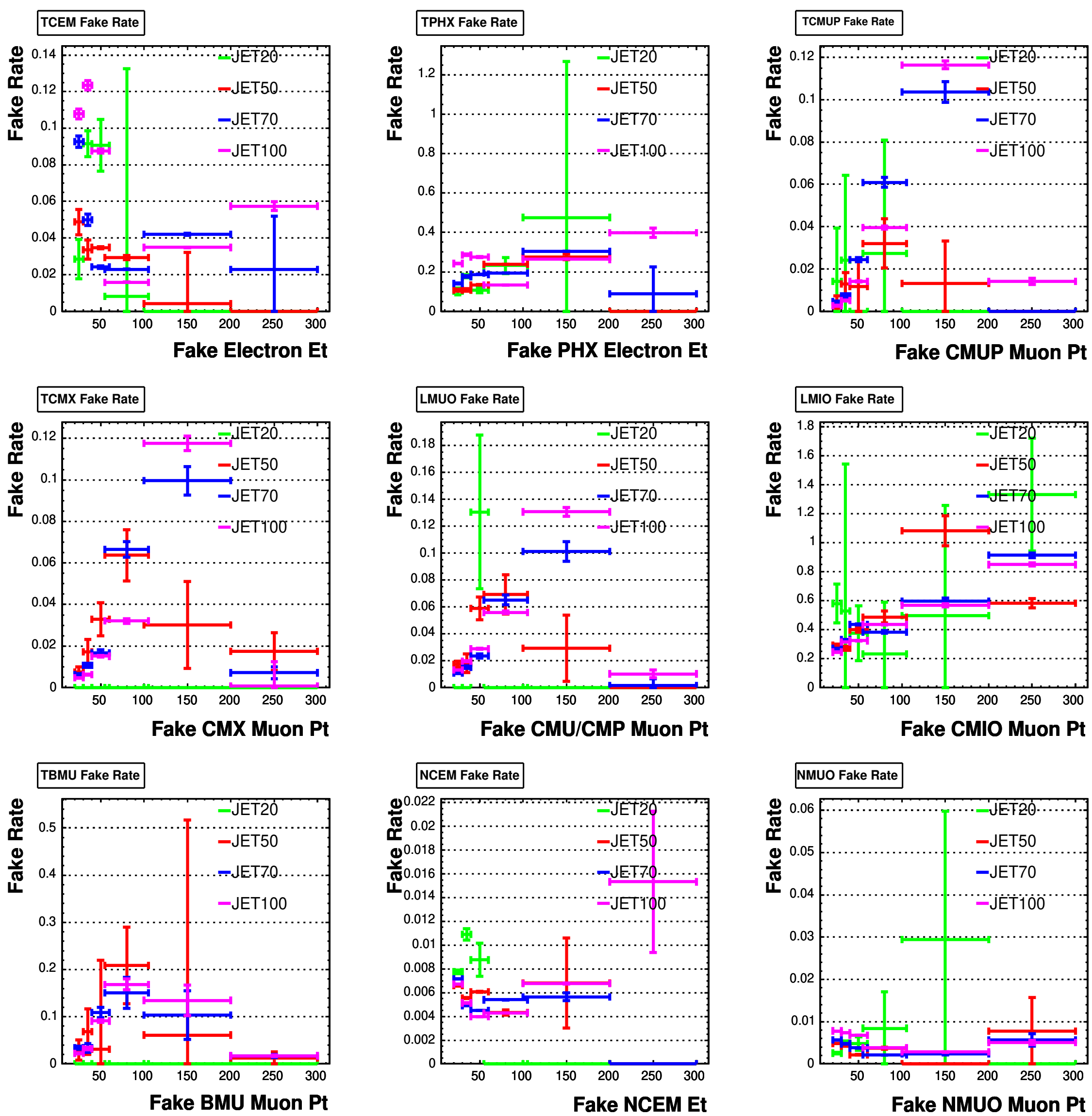

Figure 12: Fake rate estimates versus lepton p_T for each fakeable category in the date period 26 $\sim$ 28. The JET50 fake rates, shown in red, are compared to the JET20 (green), JET70 (blue) and JET100 (magenta) fake rates. TBMU fakeable objects are not used in this analysis.

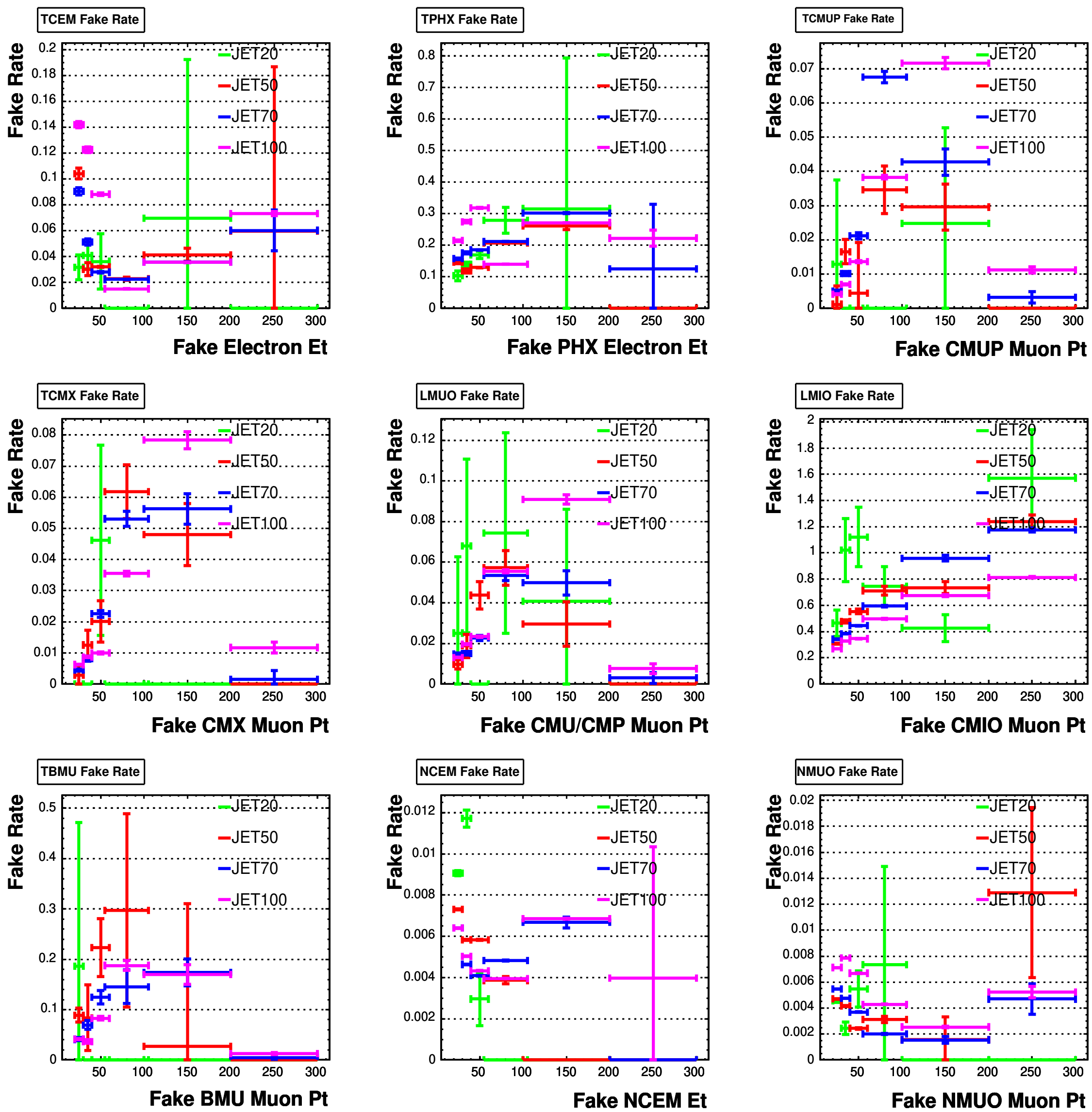

Figure 13: Fake rate estimates versus lepton p_T for each fakeable category in the date period 29 $\sim$ 31. The JET50 fake rates, shown in red, are compared to the JET20 (green), JET70 (blue) and JET100 (magenta) fake rates. TBMU fakeable objects are not used in this analysis.

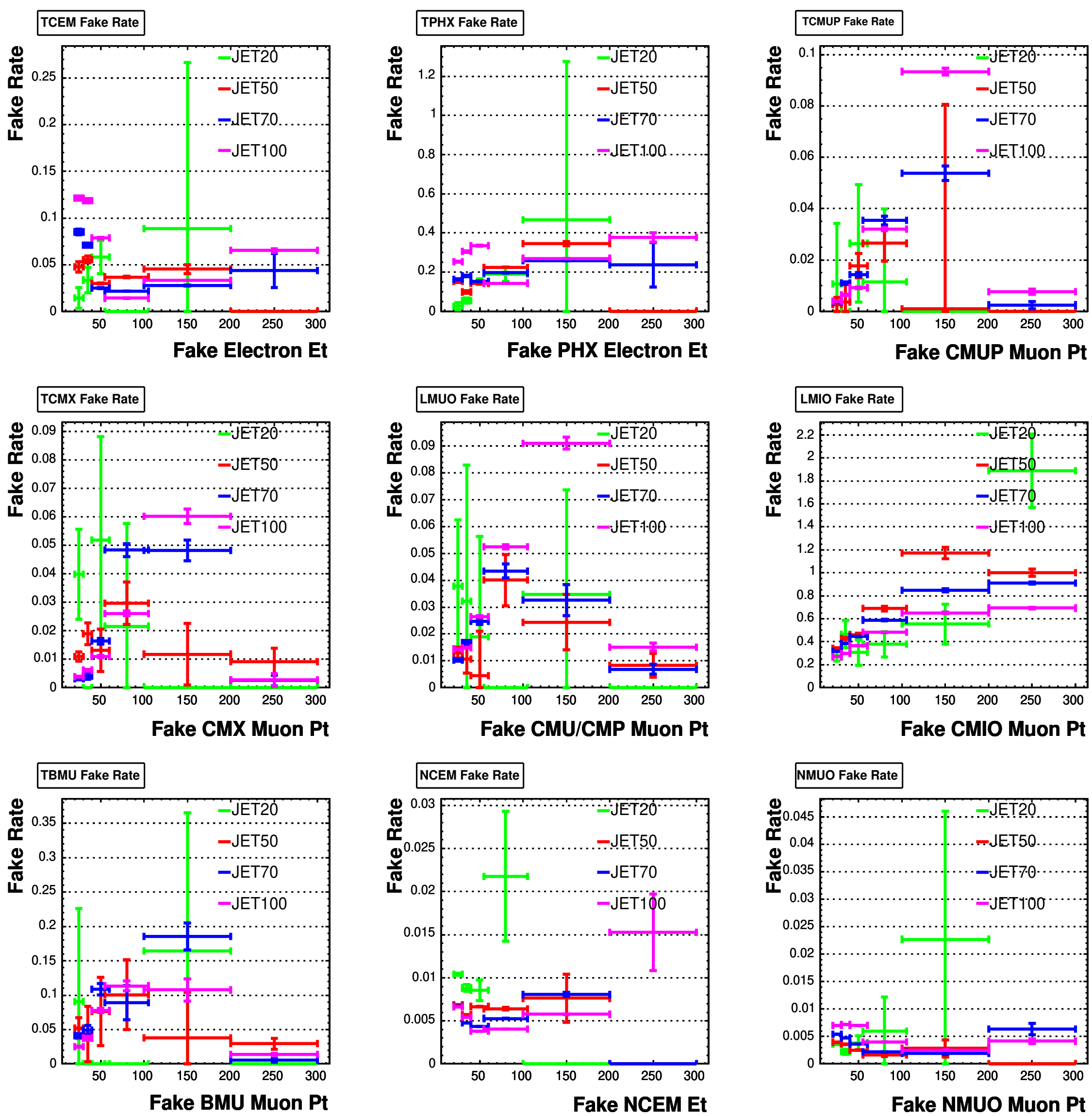

Figure 14: Fake rate estimates versus lepton p_T for each fakeable category in the date period 32 $\sim$ 34. The JET50 fake rates, shown in red, are compared to the JET20 (green), JET70 (blue) and JET100 (magenta) fake rates. TBMU fakeable objects are not used in this analysis.

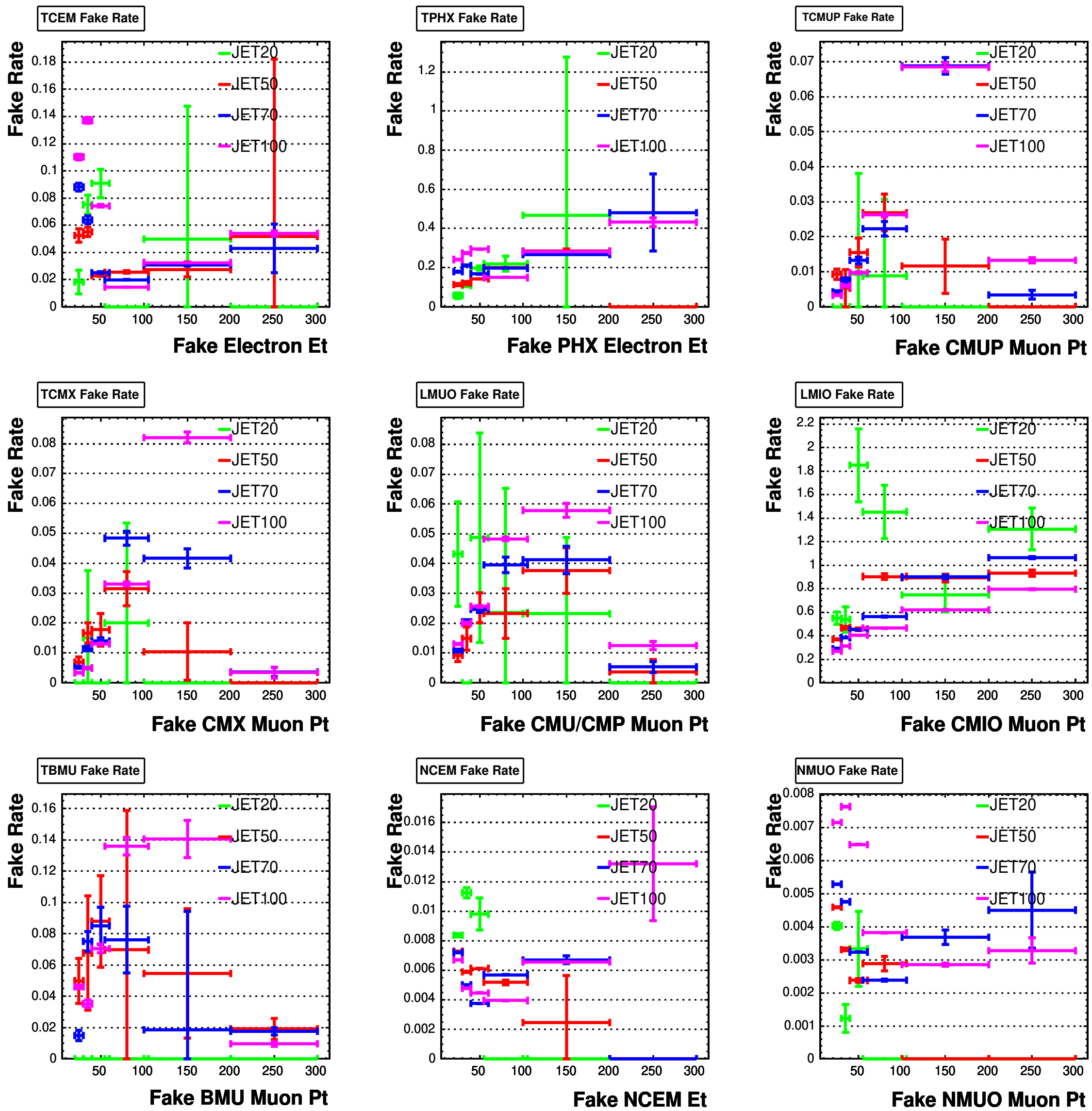

Figure 15: Fake rate estimates versus lepton p_T for each fakeable category in the date period 35 $\sim$ 38. The JET50 fake rates, shown in red, are compared to the JET20 (green), JET70 (blue) and JET100 (magenta) fake rates. TBMU fakeable objects are not used in this analysis.

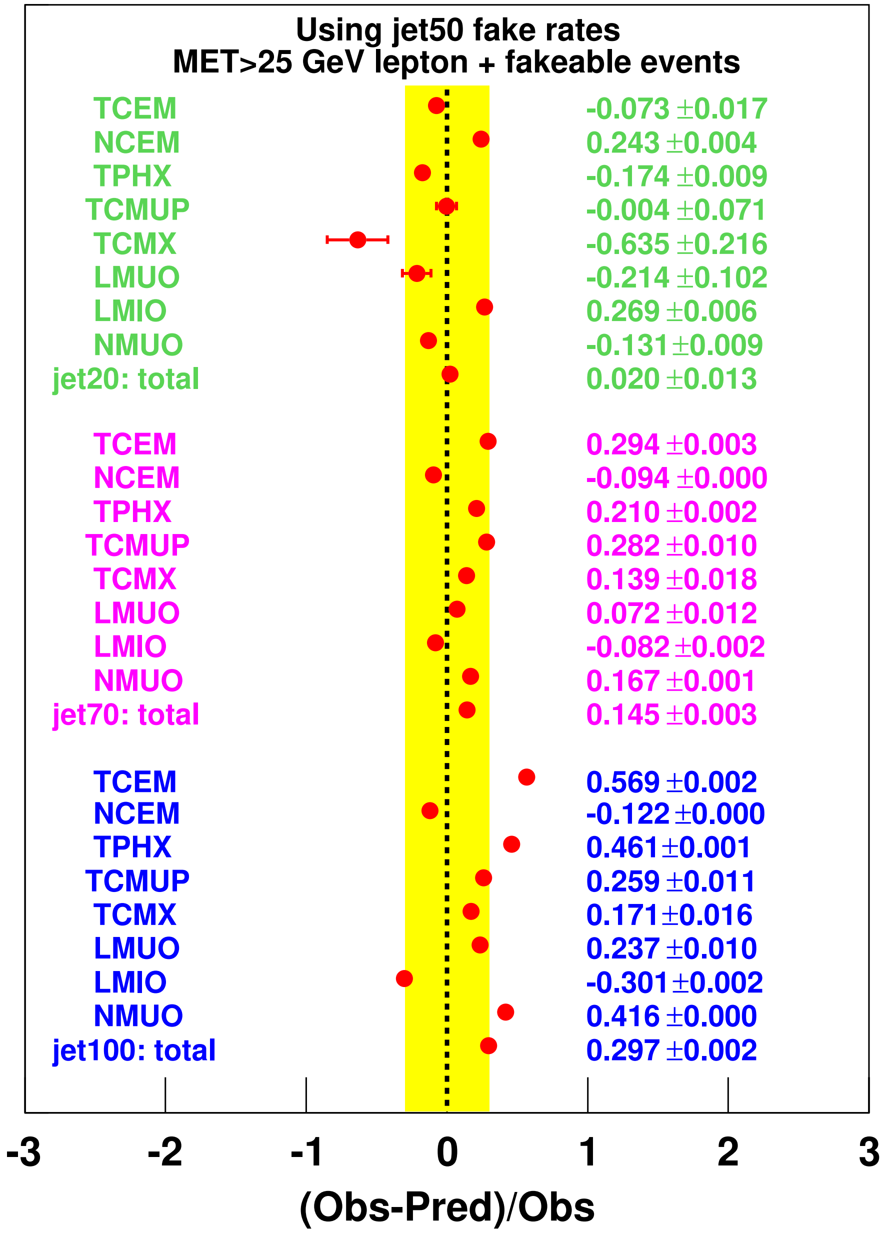

Figure 16: Ratio of observed total number of fake lepton for each fakeable category vs the JET50-based prediction. With the exclusion of the isolated electron yields in the JET20 sample, the predictability of the JET50 p_T dependent fake rate is good at the 30% level, as shown by the yellow band in the plot.

6 Systematics Studies

In this section we briefly review the systematics studies performed for the signal and backgrounds MC estimates.

A common systematics to signal and background MC estimates comes from the uncertainty on the lepton ID scale factors. These factors are measured in Z events, which have a limited jet activity. CDF-8503 limit possible systematic variations in the lepton scale factor due to extra-jet activity to 1.1%. We assign a conservative systematic of 2% to the lepton ID scale factors of table 3 and assumed that it is 100% correlated among the different MC samples. So the total lepton ID systematic uncertainty turn to be 2.2% by adding 0.1% systematic uncertainty due to the additional scale factor for CMP, CMU, CMIO.

Another common systematics comes from jet energy scale uncertainties. This is measured using the change in the default acceptance obtained from shifting the jet corrections up and down by 1σ of their systematic uncertainty. Although the central value for this systematic source is calculated separately for each MC background sample and, within each sample, for each jet multiplicity bin (see Table 15), a 100% correlation is assumed when propagating this systematic uncertainty to final cross section.

A final source of correlated systematic, this time affecting only MC-based backgrounds, is the uncertainty on the N_{jet} scale factor.

Source	0j(%)	1j(%)	$\geq$ 2j(%)	H_T, OS(%)
`ttop25`	30.0	13.3	2.6	3.3
`DY/`$Z \to \tau\tau$`(ALPGEN)`	7.3	15.4	22.5	16.3
`ihht1a`	3.2	7.3	19.1	17.9
`jhht1a`	6.1	2.1	14.3	15.2
`khht1a`	3.6	3.0	12.7	12.5
`rewk28/29`	2.7	5.6	10.0	10.0

Table 15: Systematics uncertainties, as percentage of the raw Monte Carlo acceptance, due to JES systematic variation for the different Standard Model processes.

Uncorrelated sources of systematic uncertainties are the jet fake systematics, the cross section uncertainties and a 30% systematic uncertainty on the conversion rejection scale factor. For the signal acceptance, we estimated systematic uncertainties due to multiple effects: MC generator, ISF/FSR variations, PDF's uncertainty and Color reconnection. The first two components are calculated by comparing the raw MC acceptance of the default $t\bar{t}$sample (`ttop25`) to specialized MC samples. Details on the PDF's uncertainty calculation are contained in the next section. And the systematics uncertainty due to the Color reconnection(CR) is just added in this analysis. We compare two different CR sample such ad Tune Apro (`ctopsd`) and the Tune ACRpro (ctopse). A summary tables of the systematic uncertainties affecting the $t\bar{t}$ acceptance is shown in Table 16.

Source	Systematic Error (%)
$t\bar{t}$ signal acceptace : 4.8	
Lepton ID	2.2
MC Generator	1.9
ISR/FSR	1.3
PDF's	0.6
Color Reconnection	1.2
Jet corrections	3.3
Background modeling	
Lepton ID	2.2
Njet scale factor	5.1
Jet corrections	
($WW/WZ/ZZ$)	17.9/15.2/12.5
($DY/Z \to \tau\tau$)	16.3
($DY/Z \to ee\mu\mu$)	5
($W\gamma$)	10.0
Fake rate	30
Total	8.6

Source	Systematic Error (%)
$t\bar{t}$ signal acceptace : 6.9	
Lepton ID	2.2
MC Generator	1.9
ISR/FSR	1.3
PDF's	0.6
Color Reconnection	1.2
Jet corrections	3.3
b-tagging	5.0
Background modeling	
Lepton ID	2.2
Njet scale factor	5.1
Jet corrections	
($WW/WZ/ZZ$)	17.9/15.2/12.5
($DY/Z + LF$)	5.5
($DY/Z + HF$)	9.4
($W\gamma$)	10.0
Fake rate	30
Mistag Matrix	9.4
Heavy Flavor SF	7.7
Total	7.2

Table 16: The left table shows Summary of systematic uncertainties for pretag events and the right table for b-tagged events.

6.1 Systematics due to PDF uncertainties

The CTEQ5L parton distribution function (PDF) are used in the default "ttop25" PYTHIA sample. To evaluate the systematics due to PDF uncertainties, we calculate the acceptance variation from the default acceptance when we use different PDF sets, namely MRST72, MRST75, CTEQ6L, CTEQ6L1 and CTEQ6M. To calculate the dependence of the acceptance on the different PDF sets, we adopt the weighted MC method [8]. In this method, we reweigh each event of a MC sample we already have, instead of generating a different set of MC events for each different PDF sets. We first obtain the parton momentum fractions x_1 and x_2 and Q^2 for each $t\bar{t}$ MC event, next we calculate the relative probability of the event for the PDF set we are considering by dividing it by the probability of the same event for the default PDF set (CTEQ5L). We use the relative probability as a weight for each event, and the sum of these weights for accepted events over the sum of the weights for the whole generated sample gives a rough estimate of the acceptance with each different PDF set. Table 17 summarizes the resulting acceptances and variations from the default acceptance using CTEQ5L.

We estimate the effect of different PDF set to be $\pm 0.1441\%$ by comparing the acceptance of MRST72 with CTEQ5L which gives the largest effect on the acceptance in the table. Likewise, we estimate the effect of α_s uncertainty to be $\pm 0.1633\%$ by comparing MRST72 with MRST75.

PDF	Acceptance(%)	Difference(%)	Description
CTEQ5L	0.7558	—	default PDF set
MRST72	0.7568	0.1441	default MRST
MRST75	0.7581	0.3076	MRST lower α_s
CTEQ6L	0.7567	0.1289	different α_s
CTEQ6L1	0.7561	0.0450	different α_s
CTEQ6M	0.7570	0.1686	

Table 17: Signal acceptance for different PDF sets evaluated using the weighted MC method. Differences from the default "ttop25" acceptance using CTEQ5L are also listed.

In the next step, we estimate the effect due to the variation of 20 independent parameters of the CTEQ6M PDF fit. We evaluate the acceptance, calculated using the weighted MC method as well, by shifting up and down by 1σ the uncertainties of 20 eigenvector directions within CTEQ6M. Table 18 summarizes the central value for the acceptances using the weighted MC method and its percentage difference with respect to the default CTEQ6M acceptance for each of the 20 eigenvector shifts.

The sum in quadrature of the all of the positive and negative variations gives us a value of $+0.2938\%$ and -0.5730%, respectively, for the systematic uncertainty due to uncertainties in 20 parameters of PDF.

The sum in quadrature of the systematics from the uncertainty of MRST, α_s, and 20 parameters is $+0.3363\%$ to the positive side and -0.5960% to the negative side. We quote 0.596% which is larger one as the systematic due to PDF uncertainties.

7 Background and Signal Tables

7.1 Pretag Signal Candidate events

The first step in validating the top DIL selection for the 9.1 fb^{-1} analysis is to produce the background tables for the 0-jet and 1-jet control bins, using a cut on MetSig cut as a Z-veto rejection tool. The results are shown in Tables 19. In general we see excellent agreement between data and predictions which give us confidence in the predictability of the methods used to calculate the backgrounds for high $\not\!\!E_T$ events

Eigenvector index	Acceptance(%) $+1\sigma$ up	Diff.(%)	Acceptance(%) -1σ down	Diff.(%)
# 1	0.7573	0.0400	0.7567	-0.0402
# 2	0.7570	-0.0073	0.7571	0.0073
# 3	0.7571	0.0136	0.7569	-0.0122
# 4	0.7570	-0.0021	0.7571	0.0029
# 5	0.7569	-0.0120	0.7571	0.0116
# 6	0.7577	0.0897	0.7564	-0.0893
# 7	0.7561	-0.1234	0.7579	0.1115
# 8	0.7583	0.1705	0.7559	-0.1515
# 9	0.7576	0.0756	0.7565	-0.0687
# 10	0.7574	0.0511	0.7566	-0.0507
# 11	0.7570	-0.0091	0.7570	-0.0083
# 12	0.7566	-0.0609	0.7570	-0.0058
# 13	0.7576	0.0819	0.7562	-0.1108
# 14	0.7574	0.0460	0.7569	-0.0141
# 15	0.7580	0.1232	0.7534	-0.4763
# 16	0.7566	-0.0503	0.7568	-0.0366
# 17	0.7569	-0.0129	0.7565	-0.0730
# 18	0.7571	0.0151	0.7572	0.0166
# 19	0.7560	-0.1378	0.7570	-0.0079
# 20	0.7567	-0.0489	0.7573	0.0402

Table 18: Signal acceptance using the the CTEQ6M PDF's shifted up and down by 1σ along 20 eigenvector directions. Each acceptance is evaluated using the weighted MC method. The percentage difference with respect to the CTEQ6M central value acceptance of 0.7570% is also listed.

dilepton events. Figures 19 show the $t\bar{t}$ and background prediction, overlaid to the data, for some kinematic distributions of events in the 0-jet and 1-jet bin, respectively.

Secondly, Table 20 give number of 2 jet bin before the H_T and the opposite lepton charge requirement. Figures 20 show the $t\bar{t}$ and backgorund prediction of this region.

Finally, Tables 21 give the observed number of DIL candidate events versus the background and $t\bar{t}$ signal expectations for the full 9.1 fb^{-1} samples. The total SM expectation is well in agreement with the observed 343 events for the 9.1 fb^{-1}respectively. Figures 21 show the $t\bar{t}$ and background prediction, overlaid to the data, for some candidate events kinematic distributions.

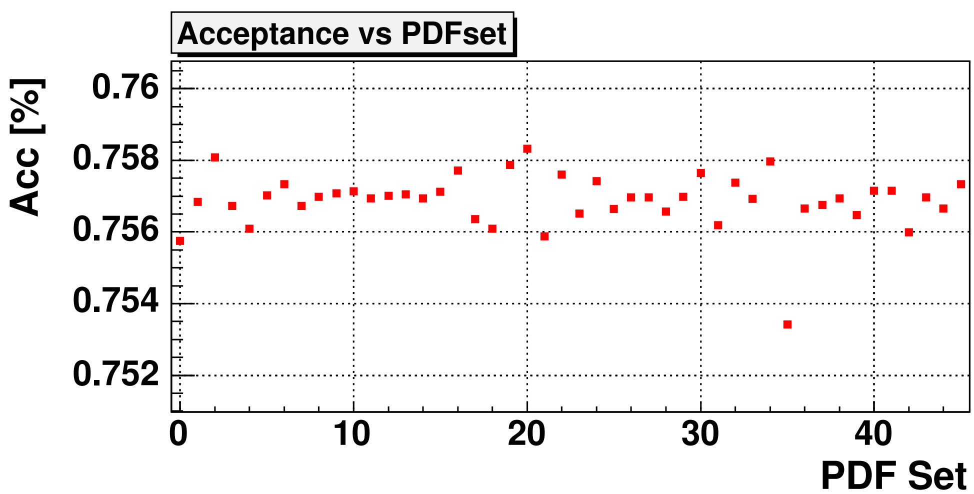

Figure 17: Measured acceptance in the 46 PDF-weighted ttop25 samples. The first point shows the default CTEQ5L's acceptance. And from 2nd to 6th points are for MRST72, MRST75, CTEQ6L, CTEQ6L1, CTEQ6M PDF set. From 7th to 46th points are corresponding to the PDF sets which have the 20 different eigenvector shifts with respect to the default CTEQ6M.

CDF II preliminary (9.1 fb^{-1})

N$jet = 0$ $t\bar{t}$ Control Sample before H_T and opposite lepton charge requirement				
Source	ee	$\mu\mu$	eμ	$\ell\ell$
WW	101.45±8.96	75.21±6.65	204.50±17.94	381.15±33.34
WZ	8.26±0.76	10.38±0.94	10.91±0.99	29.55±2.63
ZZ	12.01±0.92	10.15±0.78	1.09±0.11	23.25±1.74
Wγ	45.66±15.67	0.00±0.00	42.95±8.20	88.60±22.52
DY$\rightarrow \tau\tau$	3.90±1.33	4.38±1.42	8.66±2.20	16.94±3.19
DY$\rightarrow ee + \mu\mu$	91.10±10.11	32.02±4.63	27.41±5.85	150.53±14.82
Fakes	53.63±16.20	74.88±23.22	130.66±39.61	259.17±67.35
Total background	316.01±37.08	207.03±26.01	426.17±49.27	949.21±98.75
$t\bar{t}$ ($\sigma = 7.4$ pb)	0.64±0.08	0.43±0.06	1.10±0.11	2.17±0.17
Total SM expectation	316.65±37.11	207.45±26.03	427.28±49.32	951.38±98.85
Observed	310	275	420	1005

CDF II preliminary (9.1 fb^{-1})

N$jet = 1$ $t\bar{t}$ Control Sample before H_T and opposite lepton charge requirement				
Source	ee	$\mu\mu$	eμ	$\ell\ell$
WW	22.59±2.54	17.73±2.00	47.01±5.20	87.33±9.59
WZ	13.30±0.94	6.34±0.46	10.60±0.75	30.25±2.07
ZZ	4.07±0.33	3.77±0.30	2.39±0.20	10.23±0.76
Wγ	10.96±4.37	0.00±0.00	13.43±3.42	24.39±6.80
DY$\rightarrow \tau\tau$	14.59±2.72	12.73±2.59	28.52±5.16	55.84±9.64
DY$\rightarrow ee + \mu\mu$	83.80±13.80	35.97±6.21	15.63±3.30	135.40±21.45
Fakes	40.58±12.27	52.14±16.03	177.87±53.75	270.58±73.56
Total background	189.89±26.15	128.66±19.27	295.45±56.02	614.01±87.97
$t\bar{t}$ ($\sigma = 7.4$ pb)	13.74±0.74	12.12±0.65	29.98±1.51	55.85±2.74
Total SM expectation	203.63±26.78	140.78±19.83	325.44±57.43	669.85±90.60
Observed	225	171	316	712

Table 19: Summary tables for the 9.1 fb^{-1} Inclusive DIL sample. The top and bottom tables show the total number of background, SM expectation and data candidate events, divided by lepton flavor contribution, for 0 and 1 jet bins. The quoted uncertainties are the sum of the statistical and systematics uncertainty.

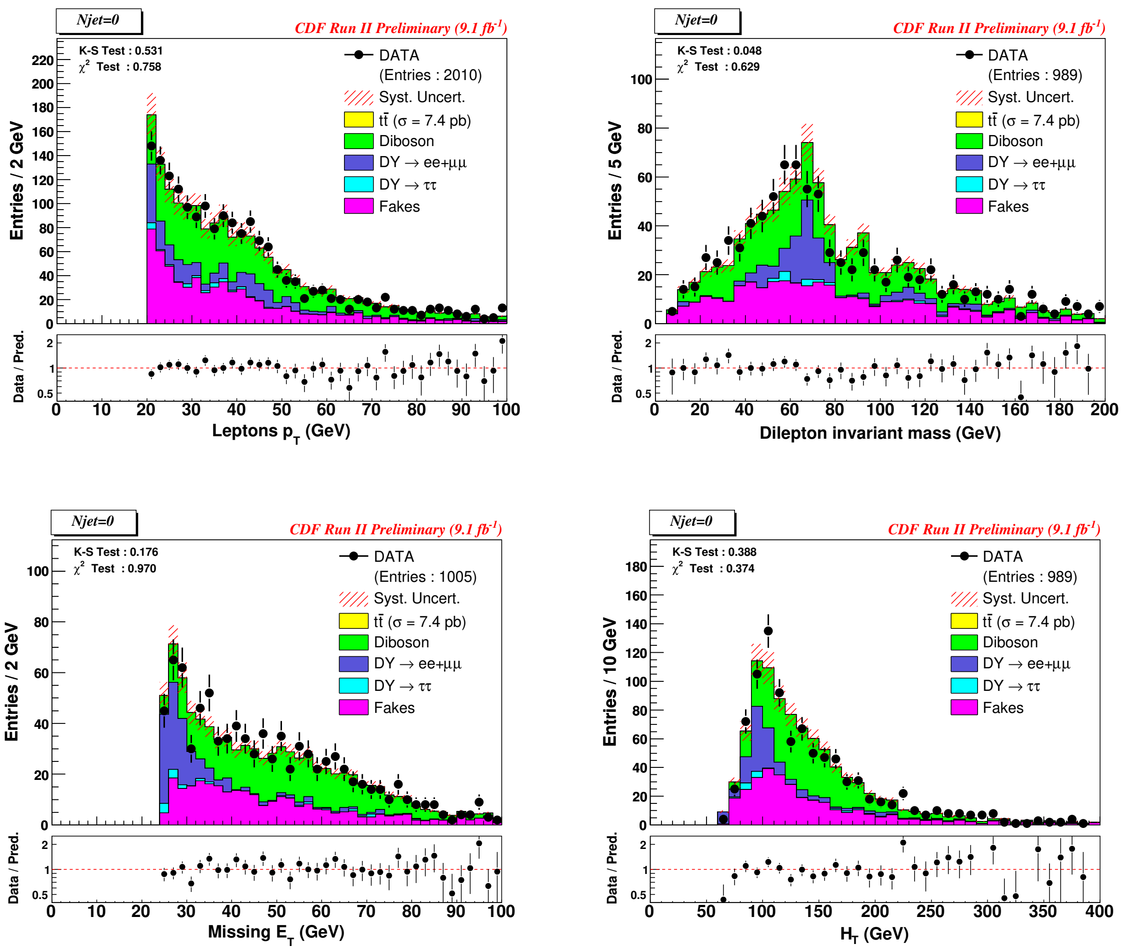

Figure 18: From top left to bottom right: background and top signal predictions, overlaid to data, for the lepton transverse energy spectrum, the dilepton invariant mass, $\not\!\!E_T$, H_T and jet transverse energy distributions in 9.1 fb^{-1} 0-jet events.

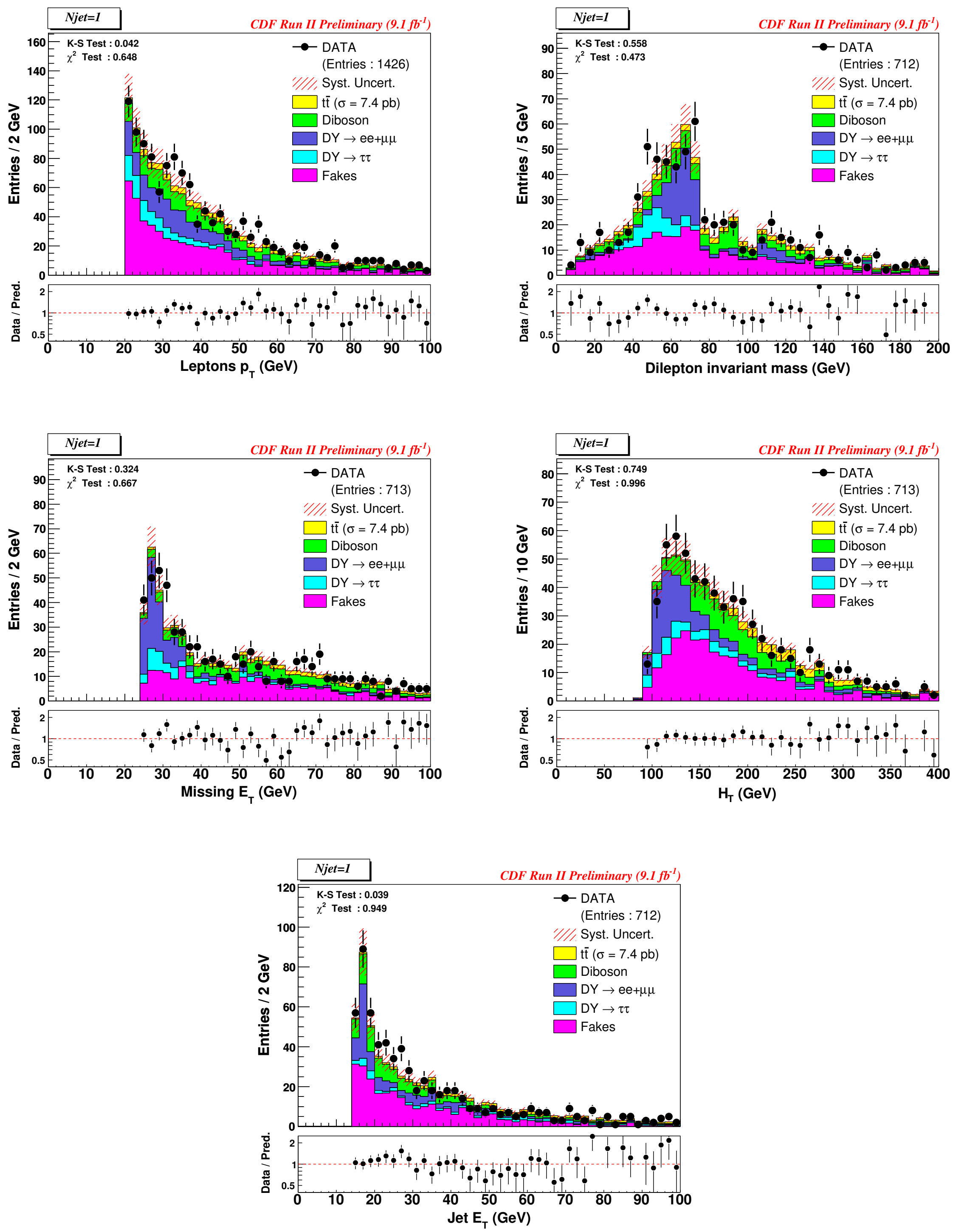

Figure 19: From top left to bottom right: background and top signal predictions, overlaid to data, for the lepton transverse energy spectrum, the dilepton invariant mass, $\not{E}_T$, H_T and jet transverse energy distributions in 9.1 fb^{-1} 1-jet events.

CDF II preliminary (9.1 fb^{-1})

N$jet \geq 2$ $t\bar{t}$ Control Sample before H_T and opposite lepton charge requirement				
Source	ee	$\mu\mu$	eμ	$\ell\ell$
WW	7.88±1.68	5.77±1.24	15.89±3.34	29.55±6.18
WZ	4.48±0.72	2.17±0.35	3.82±0.61	10.47±1.65
ZZ	2.25±0.34	1.60±0.24	1.36±0.21	5.21±0.76
Wγ	1.99±1.33	0.00±0.00	3.92±1.65	5.90±2.33
DY$\rightarrow \tau\tau$	9.32±2.27	9.40±2.27	21.02±5.05	39.74±9.37
DY$\rightarrow ee + \mu\mu$	51.19±13.75	29.96±8.29	10.01±2.73	91.15±24.14
Fakes	33.21±10.07	55.17±16.85	172.55±52.10	260.93±71.41
Total background	110.31±21.66	104.08±20.75	228.57±53.57	442.96±83.44
$t\bar{t}$ ($\sigma = 7.4$ pb)	106.31±5.14	97.52±4.71	236.66±11.31	440.49±20.98
Total SM expectation	216.62±26.64	201.60±25.30	465.23±64.75	883.45±104.25
Observed	232	217	437	886

Table 20: Summary tables for the 9.1 fb^{-1} Inclusive DIL sample. The top/bottom table shows the total number of background, SM expectation and data candidate events, divided by lepton flavor contribution, 2 jet bins before the H_T and the opposite lepton charge requirement events. The quoted uncertainties are the sum of the statistical and systematics uncertainty.

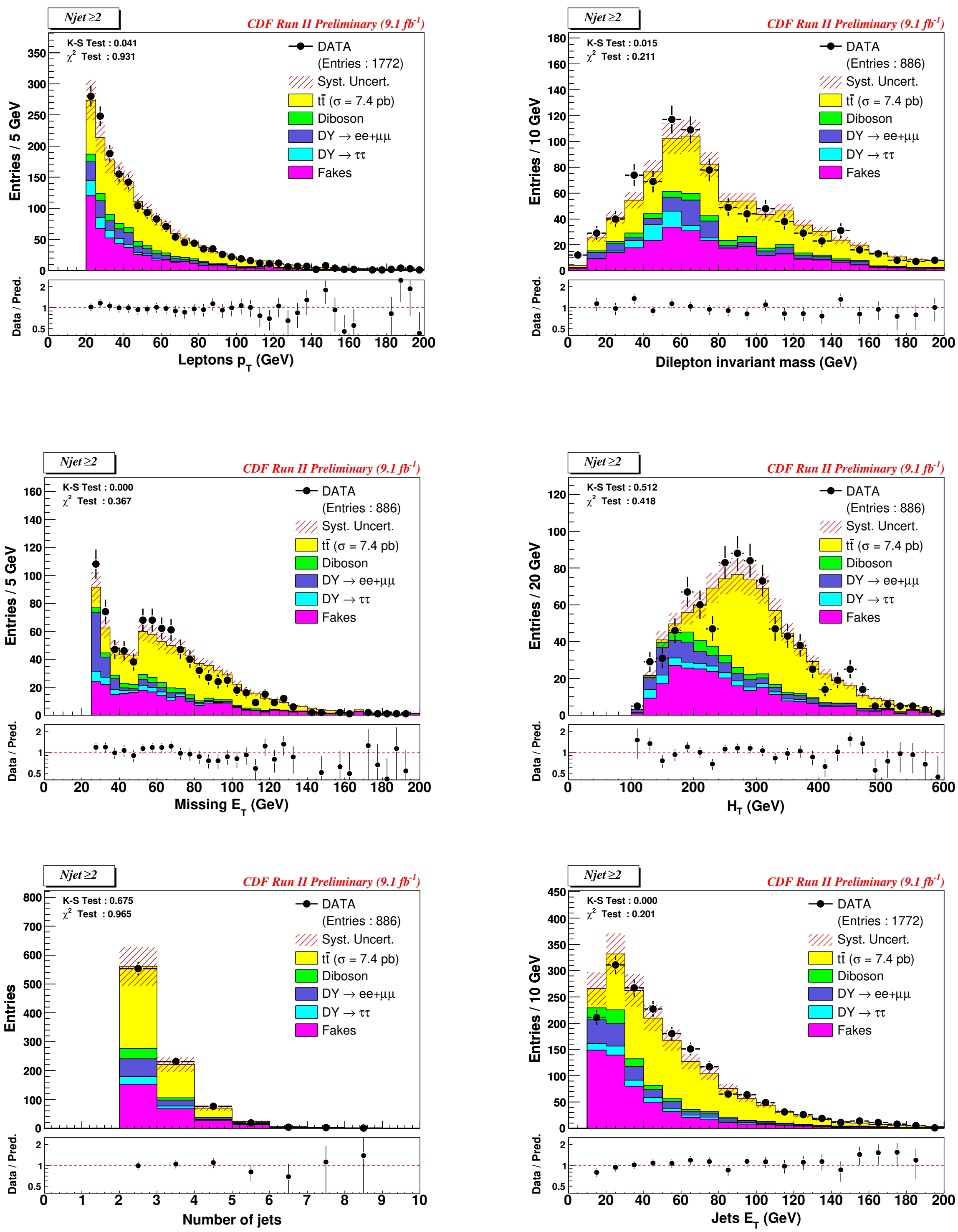

Figure 20: From top left to bottom right: background and top signal predictions, overlaid to data, for the lepton transverse energy spectrum, the dilepton invariant mass, $\not{E}_T$, H_T, jet multiplicity and jet transverse energy distributions in 9.1 fb^{-1} 2-jet before the H_T and the opposite lepton charge requirement events.

CDF II preliminary (9.1 fb^{-1})

$t\bar{t}$ Signal Events per Dilepton Flavor Category before b-tagging				
Source	ee	$\mu\mu$	eμ	$\ell\ell$
WW	5.03±1.04	3.90±0.81	9.23±1.86	18.16±3.61
WZ	2.62±0.45	1.56±0.27	1.52±0.27	5.70±0.96
ZZ	1.71±0.26	1.30±0.20	0.68±0.11	3.69±0.54
Wγ	0.73±0.77	0.00±0.00	0.00±0.00	0.73±0.77
DY$\rightarrow \tau\tau$	5.30±1.04	5.31±1.02	11.58±2.12	22.19±3.96
DY$\rightarrow ee + \mu\mu$	22.27±4.14	17.11±2.95	5.54±1.52	44.92±5.98
Fakes	12.57±3.90	23.27±7.26	67.04±20.46	102.87±28.38
Total background	50.21±6.89	52.45±8.36	95.60±21.24	198.26±31.44
$t\bar{t}$ ($\sigma = 7.4$ pb)	97.61±4.73	92.97±4.49	221.97±10.62	412.55±19.65
Total SM expectation	147.82±10.97	145.42±12.53	317.56±31.67	610.81±50.76
Observed	147	165	313	625

CDF II preliminary (9.1 fb^{-1})

Pretag Control Sample and Signal Events per Jet Multiplicity					
Source	0 jet	1 jet	≥ 2 jet	H_T	H_T, OS
WW	381.15±33.34	87.33±9.59	29.55±6.18	18.69±3.72	18.16±3.61
WZ	29.55±2.63	30.25±2.07	10.47±1.65	8.26±1.38	5.70±0.96
ZZ	23.25±1.74	10.23±0.76	5.21±0.76	4.43±0.64	3.69±0.54
Wγ	88.60±22.52	24.39±6.80	5.90±2.33	0.73±0.77	0.73±0.77
DY$\rightarrow \tau\tau$	16.94±3.19	55.84±9.64	39.74±9.37	22.64±4.04	22.19±3.96
DY$\rightarrow ee + \mu\mu$	150.53±14.82	135.40±21.45	91.15±24.14	44.92±5.98	44.92±5.98
Fakes	259.17±67.35	270.58±73.56	260.93±71.41	188.17±52.15	102.87±28.38
Total background	949.21±98.75	614.01±87.97	442.96±83.44	287.83±54.04	198.26±31.44
$t\bar{t}$ ($\sigma = 7.4$ pb)	2.17±0.17	55.85±2.74	440.49±20.98	423.57±20.17	412.55±19.65
Total SM expectation	951.38±98.85	669.85±90.60	883.45±104.25	711.41±73.98	610.81±50.76
Observed	1005	712	886	708	625

Table 21: Summary tables of background estimates, pretag $t\bar{t}$ predictions and events in 9.1 fb^{-1} Inclusive DIL sample. The top table shows the total number of background, SM expectation and data candidate events, divided by lepton flavor contribution. The bottom table shows the same contributions for each jet bin after all cuts but before the H_T and Opposite Charge requirements are applied and in the 2 jet bin after applying only the H_T cut. The last column contains the candidate events with all cuts applied. The quoted uncertainties is the sum of the statistical and systematics uncertainty.

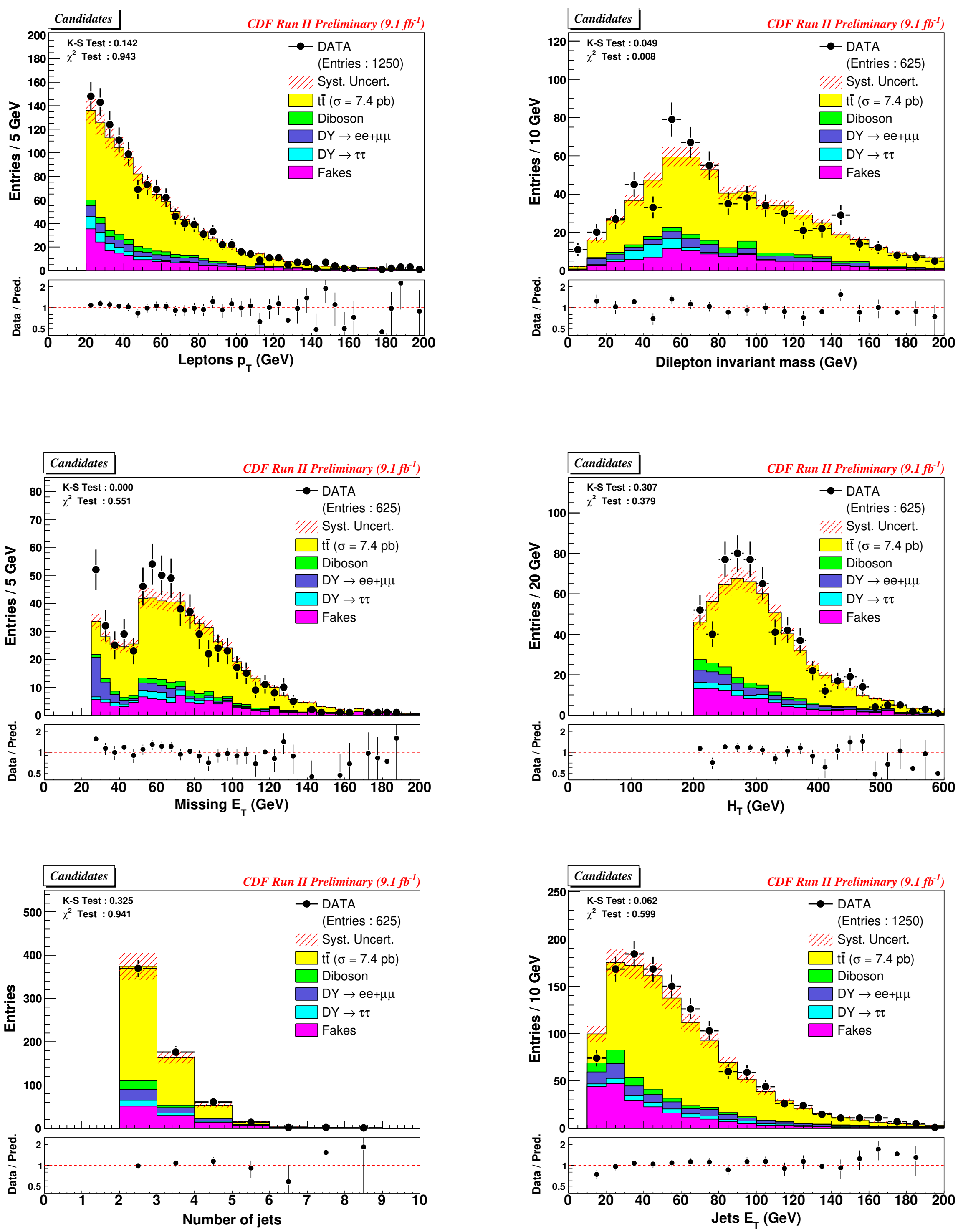

Figure 21: From top left to bottom right: background and top signal predictions, overlaid to data, for the lepton transverse energy spectrum, the dilepton invariant mass, $\not\!\!E_T$ and H_T distributions in 9.1 fb^{-1} top DIL candidate events.

7.2 b-tagged Signal Candidate events

In this section we describe how to apply Tight SecVtx b-tagging from the pretag samples. We use Method II approach to estimate the DY/Z+Light Flavor using mistag matrix applied to ALPGEN+PYTHIA Monte Carlo events. We take the mistag matrix of the "jetMistagJun2009".

We calculate the heavy flavor scale factor in the table 22. Due to technical difficulties we were not able to generate the Drell-Yan + $c\bar{c}$ events below the Z mass peak region, thus we used only $b\bar{b}$ Monte Carlo to represent DY/Z + heavey flavor events and then rescale heavy flavor background using these scale factors. For the heavy flavor rescale method, the kinematic distributions before missing E_T cut and Zveto cut are shown in Figures 22. The data is consistent with our expectation. The calculation method of the Heavey Flavor scale factor is refered from the Stop quarks search analysis in dilepton channel [9]. And the scale factor for the tight SecVtx tag is taken from CDF High P_T b-tag ground as 0.96 ± 0.05.

	1 jet	≥ 2 jet
ee	3.095±0.430	1.806±0.268
$\mu\mu$	4.033±0.565	2.403±0.362
Total	3.498±0.474	2.064±0.300

Table 22: Jet bin correction factors for Z + heavy flavor events without Z + $c\bar{c}$ events. The uncertainty on the total scale factor takes into account statistical uncertainty added in quadrature to half of the discrepancy between ee and $\mu\mu$ channels.

Table 23, Figures 23 and Table 24, Figures 24 show the signal and background after SecVtx b-tagging for 1-jet control events and signal candidate events respectively. We use the tight SecVtx b-tagging scale fator 0.96 ± 0.05 from CDF high p_T b-tag group.

When we apply the b-tagging, the total background number 198.26 ± 31.44 in the pretag signal candidates is significantly reduced by 17.41 ± 3.20, while the total signal candidate is predicted by 233.88 ± 16.17. Thus signal-to-background ratio is about 16:1 and we observed pure top signal candidates of 254 events from data after b-tagging.

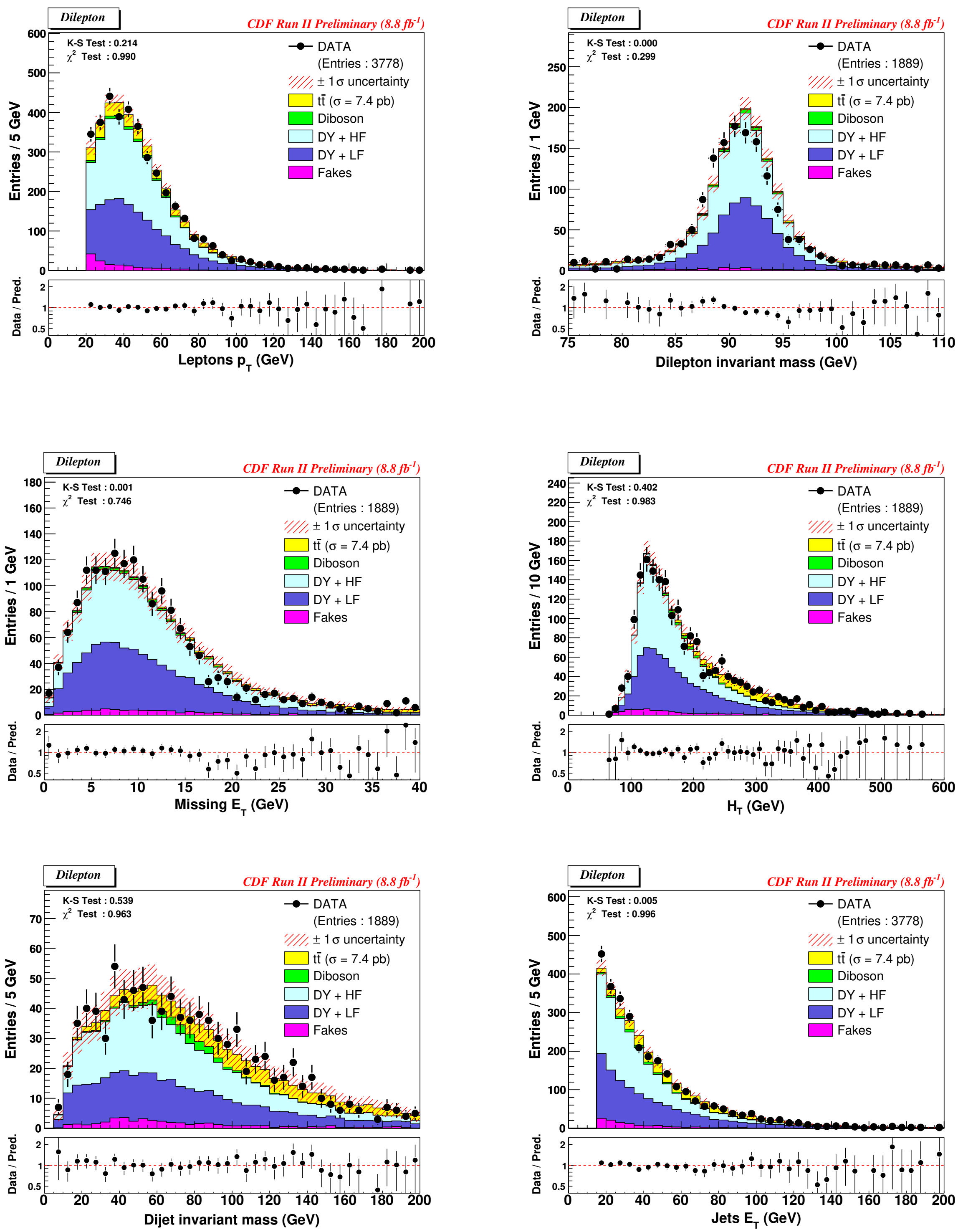

Figure 22: From top left to bottom right: background and top signal predictions, overlaid to data, for the lepton transverse energy spectrum, the dilepton invariant mass, $\not{E}_T$, H_T, jet multiplicity and jet transverse energy distributions in 8.8 fb^{-1} top DIL signal candidate events with the tight SecVtx b-tag.

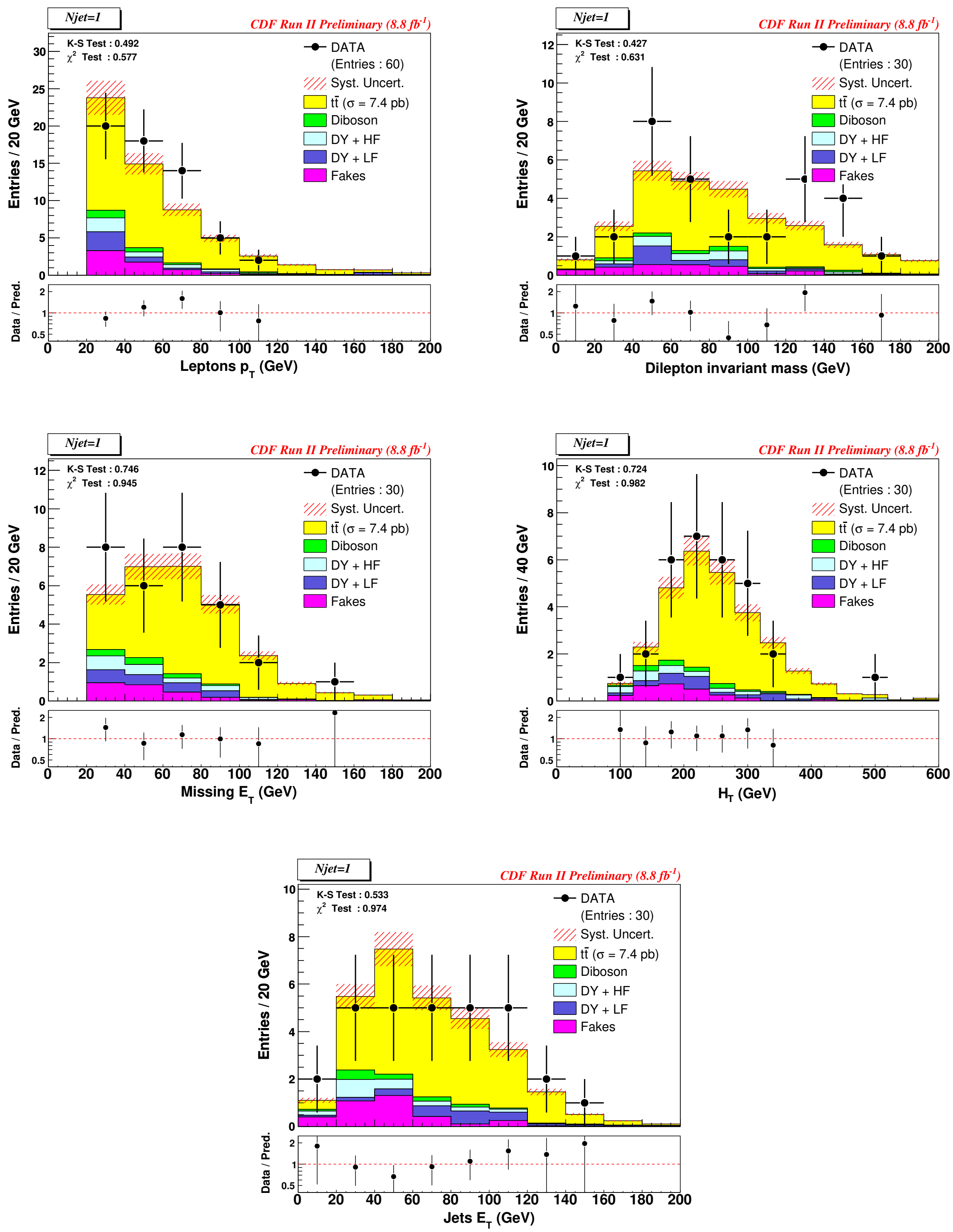

Figure 23: From top left to bottom right: background and top signal predictions, overlaid to data, for the lepton transverse energy spectrum, the dilepton invariant mass, $\not\!\!E_T$, H_T and jet transverse energy distributions in 8.8 fb^{-1} 1-jet b-tagged evensts.

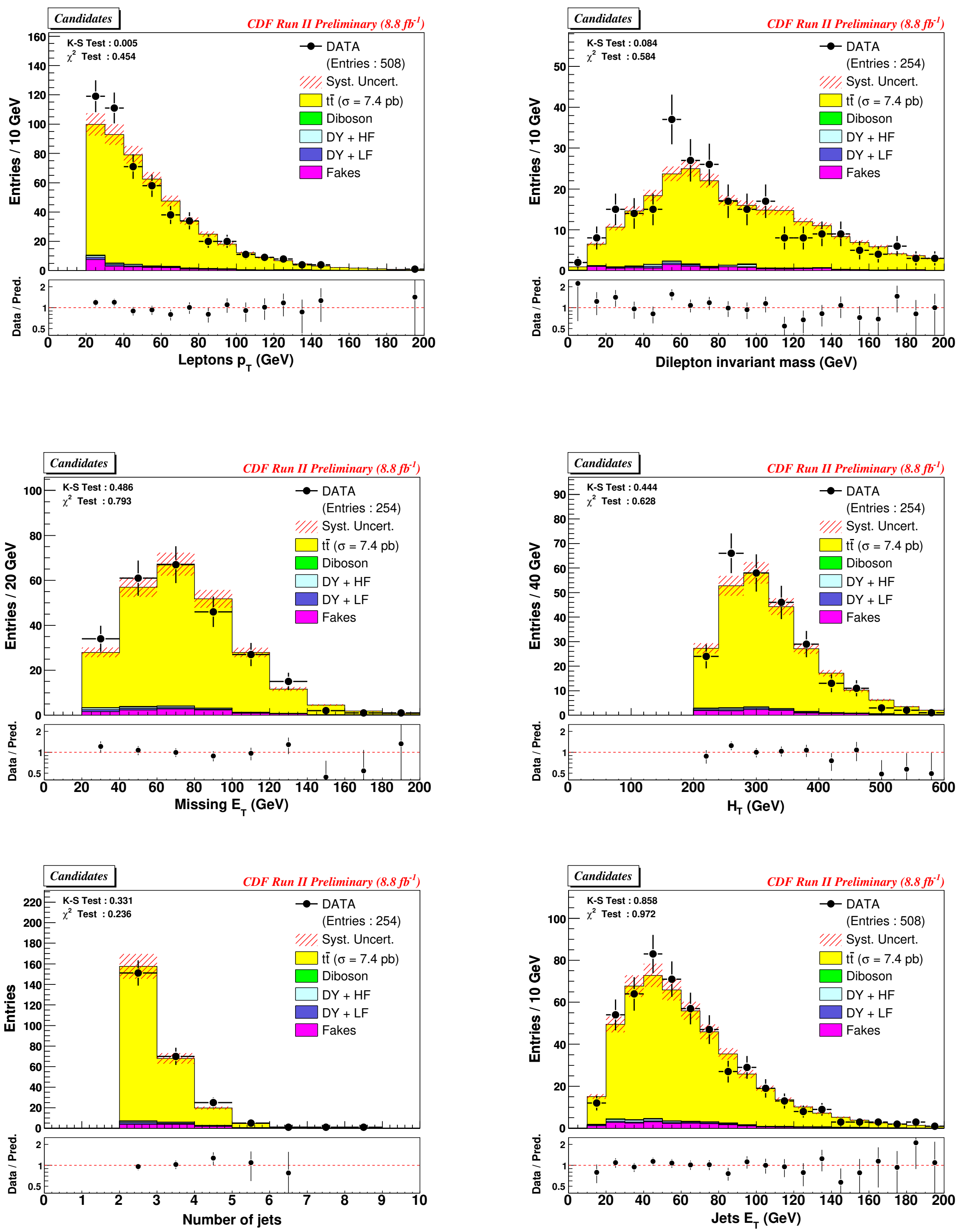

Figure 24: From top left to bottom right: btagged background and top signal predictions before the missing E_T cut and Zveto cut, overlaid to data, for the lepton transverse energy spectrum, the diljet invariant mass, $\not\!\!E_T$, H_T, jet multiplicity and jet transverse energy distributions in 8.8 fb^{-1} top DIL signal candidate events with b-tag.

CDF II preliminary (8.8 fb^{-1})

N$jet = 1$ Control Sample with the tight SecVtx b-tag				
Source	ee	$\mu\mu$	eμ	$\ell\ell$
WW	0.21±0.06	0.21±0.06	0.38±0.09	0.80±0.15
WZ	0.05±0.02	0.07±0.02	0.04±0.01	0.17±0.03
ZZ	0.04±0.02	0.04±0.01	0.01±0.01	0.10±0.02
DY+LF	1.06±0.15	0.34±0.06	0.73±0.08	2.12±0.23
DY+HF	0.84±0.14	0.52±0.09	0.51±0.11	1.87±0.29
Fakes	0.37±0.16	1.32±1.08	1.94±0.70	3.63±1.47
Total background	2.57±0.33	2.51±1.09	3.61±0.74	8.69±1.59
$t\bar{t}$ ($\sigma = 7.4$ pb)	5.18±0.42	4.76±0.38	11.13±0.82	21.07±1.51
Total SM expectation	7.75±0.69	7.27±1.27	14.74±1.47	29.76±2.85
Observed	8	11	11	30

Table 23: Top table of background estimates, $t\bar{t}$ predictions and observed events in data corresponding to an integrated luminosity of 8.8 fb^{-1} for 1 jet control sample with SecVtx b-tagging before H_T and opposite lepton charge requirement The quoted uncertainties are the sum of the statistical and systematics uncertainty.

CDF II preliminary (8.8 fb^{-1})

$t\bar{t}$ Signal Events with the tight SecVtx b-tag				
Source	ee	$\mu\mu$	eμ	$\ell\ell$
WW	0.13±0.06	0.14±0.05	0.33±0.10	0.60±0.16
WZ	0.04±0.02	0.05±0.02	0.05±0.02	0.13±0.03
ZZ	0.14±0.03	0.12±0.03	0.03±0.01	0.29±0.06
DY+LF	1.07±0.12	1.17±0.15	0.56±0.06	2.80±0.31
DY+HF	0.99±0.17	1.34±0.22	0.50±0.10	2.83±0.45
Fakes	1.88±0.69	2.16±0.85	6.72±2.16	10.76±3.06
Total background	4.24±0.76	4.99±0.94	8.19±2.18	17.41±3.20
$t\bar{t}$ ($\sigma = 7.4$ pb)	55.64±3.90	52.02±3.64	126.23±8.76	233.88±16.17
Total SM expectation	59.88±4.55	57.01±4.42	134.41±10.80	251.29±19.21
Observed	53	71	130	254

Table 24: Summary table by lepton flavor content with SecVtx b-tagging, of background estimates, $t\bar{t}$ predictions and observed events in data corresponding to an integrated luminosity of 8.8 fb^{-1} for $t\bar{t}$ signal events. The quoted uncertainties are the sum of the statistical and systematics uncertainty.

8 Results

For pretag signal candidate events, using the numbers in Table 21 for the numerator and the denominator quoted in Section 4, we measure:

$$\sigma_{t\bar{t}} = 7.66 \pm 0.46 \pm 0.66 \pm 0.47 \text{ pb} \tag{7}$$

for the 9.1 fb^{-1} data sample, after propagating the acceptance and background systematics uncertainties.

The last error is 6% uncertainty coming from luminosity measurement.

For b-tagged signal candidate events, using the numbers in Table 24, we measure:

$$\sigma_{t\bar{t}} = 7.47 \pm 0.50 \pm 0.53 \pm 0.46 \text{ pb} \tag{8}$$

for the 8.8 fb^{-1} data sample, after propagating the acceptance and background systematics uncertainties.

In the Figure 25, the left plot shows the number of candidate events in 0, 1, $\geq$2jet events together with a histogram representing the component of the background for the pra-tagged events. And the right plot shows the number b-tagged events in 1jet control region and signal candidate events. The yellow band gives the $\mathrm{t\bar{t}}$ contribution for a cross section of 7.4 pb. The red hatched area is the uncertainty in the total background estimate.

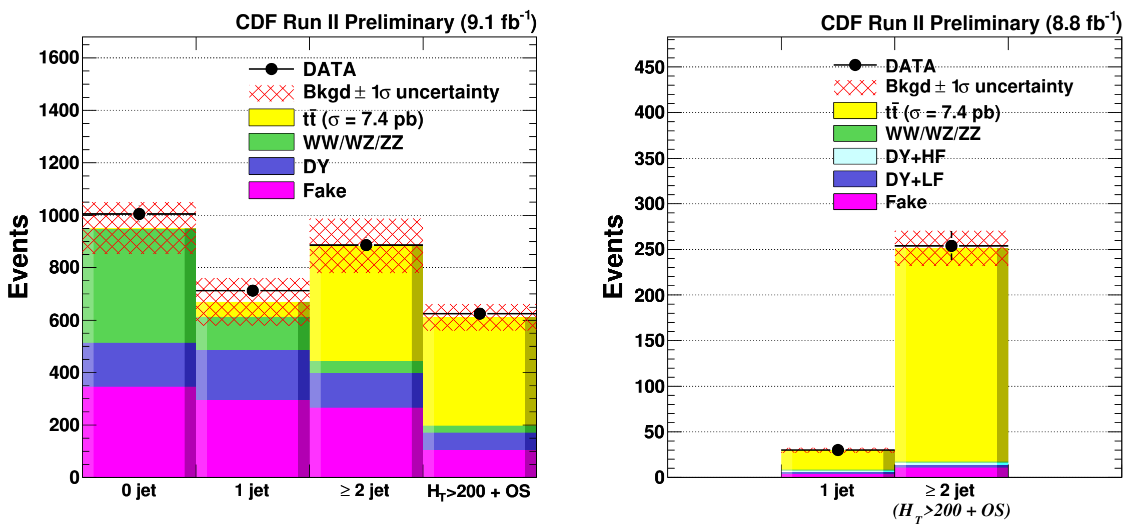

Figure 25: Observed dilepton candidate events (black point) by jet multiplicity for the pretag(Left) and b-tagged(Right) events. The colored histogram represents the background contribution for an assumed $\sigma_{t\bar{t}}$ = 7.4 pb. The red hatched area is the uncertainty in the total background estimate.

9 Conclusions

We have reported on the measurement of the $t\bar{t}$ cross section using the top DIL selection in 9.1 fb^{-1} (8.8 fb^{-1} on b-tagging) of CDF full data. The measured cross section is found to be

For 625 pretag signal candidate events:

$$\sigma_{t\bar{t}} = 7.66 \pm 0.46_{\mathrm{stat}} \pm 0.66_{\mathrm{syst}} \pm 0.47_{\mathrm{lumi}} \text{ pb.}$$

For 254 tight SecVtx b-tagged signal candidate events:

$$\sigma_{t\bar{t}} = 7.47 \pm 0.50_{\mathrm{stat}} \pm 0.53_{\mathrm{syst}} \pm 0.46_{\mathrm{lumi}} \text{ pb.}$$

References

[1] D. Goldstein *et al*, CDFNote 6588, July 2003 and CDFNote 6830, July 2004
M. Tecchio *et al*, CDFNote 8741, April 2007 and CDFNote 8040, February 2006
N. Kimura *et al*, CDFNote 9247, May 2008
C.S. Moon *et al*, CDFNote 9635, Dec 2008
C.S. Moon *et al*, CDFNote 10054, May 2010
1, 3

[2] E. J. Thomson *et al*, CDFNote 5947, October 2003
3

[3] `http://www-cdf.fnal.gov/internal/dqm/goodrun/v45/goodv45.html`
3

[4] Mark Neubauer, private communications. 5

[5] `http://www-cdf.fnal.gov/internal/physics/top/RunIITopProp/gen6Sum06/lumi_v45.html`
4

[6] `http:www-cdf.fnal.gov/~tecchio/internal/topntuple/DIL_topntuple.html`
5

[7] A. D. Martin *et al.*, Phys. Lett. B **652**, 292 (2007). 13

[8] How to estimate PDF acceptance uncertainties using Weighted MC:
`http://www-cdf.fnal.gov/internal/physics/joint_physics/instructions/PDFUncertainties/pdf.html`
36

[9] A. Ivanov *et al*, CDFNote 9417, May 2009
47

Appendix

Tables of Monte Carlo events passing each step of the top DIL selection. These tables have been obtained by runnig the "topdil" selection macro in the topana_614_v14 package, which can be downloaded at below.
`http:www-cdf.fnal.gov/~csmoon/internal/DIL/9.1fb/topcode`.

Category	ALL	Zveto	Met	L-cut	0j	1j	≥2j	Ht	OS
DIL Category	ALL	ZVET	MET	dphi	0j	1j	¿=2j	Ht	OS
CEM-CEM	11576	8952	8018	7352	41	880	6431	6202	6195
CEM-NICEM	3666	1864	1705	1567	7	114	1446	1388	1305
PHX-CEM	5617	4411	3942	3613	19	447	3147	2996	2614
PHX-NICEM	836	384	347	318	1	26	291	276	234
ee inclusive	21695	15611	14012	12850	68	1467	11315	10862	10348
ee iso-iso	17193	13363	11960	10965	60	1327	9578	9198	8809
CMUP-CMUP	4044	3425	3052	2793	14	347	2432	2356	2356
CMUP-NICMUP	1309	792	733	690	0	34	656	639	605
CMUP-CMU	1742	1455	1284	1181	5	120	1056	1027	1027
CMUP-NICMU	287	173	161	149	1	7	141	137	129
CMUP-CMP	2450	2089	1861	1687	8	189	1490	1436	1436
CMUP-NICMP	460	248	234	215	0	12	203	198	179
CMUP-CMX	4169	3539	3211	2938	7	356	2575	2467	2467
CMUP-NICMX	693	369	339	315	0	15	300	283	257
CMX-NICMUP	624	370	340	314	0	18	296	289	271
CMUP-CMIO	1589	1322	1180	1083	6	138	939	908	907
CMX-CMX	1041	869	769	702	7	83	612	594	594
CMX-NICMX	303	152	142	130	0	13	117	108	98
CMX-CMU	750	637	569	528	3	69	456	431	431
CMX-NICMU	111	64	57	53	0	3	50	43	40
CMX-CMP	1105	931	851	782	3	88	691	664	664
CMX-NICMP	190	108	102	94	0	7	87	81	74
CMX-CMIO	698	598	526	474	1	55	418	403	403
mm inclusive	21565	17141	15411	14128	55	1554	12519	12064	11938
mm iso-iso	17588	14865	13303	12168	54	1445	10669	10286	10285
CEM-CMUP	13526	12802	11326	10228	50	1213	8965	8652	8640
CEM-NICMUP	2406	1645	1506	1389	0	82	1307	1260	1195
CMUP-NICEM	2151	1311	1191	1094	4	92	998	961	896
CEM-CMU	2952	2808	2486	2254	14	233	2007	1935	1930
CEM-NICMU	511	324	292	269	0	21	248	235	219
CEM-CMP	4142	3920	3453	3120	14	367	2739	2645	2644
CEM-NICMP	874	536	482	446	2	33	411	390	355
CEM-CMX	6864	6562	5769	5224	27	645	4552	4382	4375
CEM-NICMX	1178	762	670	610	1	35	574	543	514
CMX-NICEM	931	574	515	468	0	32	436	418	389
CEM-CMIO	2505	2312	2045	1869	6	242	1621	1559	1554
PHX-CMUP	3234	3155	2749	2487	6	308	2173	2072	1821
PHX-NICMUP	533	353	321	289	1	25	263	243	195
PHX-CMX	1510	1491	1271	1140	2	138	1000	938	827
PHX-NICMX	243	160	142	134	0	12	122	116	91
em inclusive	46195	38715	34218	31021	127	3478	27416	26349	25645
em iso-iso	37071	33050	29099	26322	119	3146	23057	22183	21791
total inclusive	71852	61278	54362	49455	233	5918	43304	41667	40885
total iso-iso	89455	71467	63641	57999	250	6499	51250	49275	47931

Table 25: PYTHIA `ttop25` MC events, after each dilepton cut. The first column represents events with a good dilepton after conversion removal. The last columns gives the final number after all selection cuts.

Category	ALL	Zveto	Met	L-cut	0j	1j	≥2j	Ht	OS
CEM-CEM	6501	4880	3750	3641	2787	666	188	125	125
CEM-NICEM	715	460	373	355	201	101	53	35	35
PHX-CEM	5296	4110	3157	3040	2359	520	161	109	95
PHX-NICEM	247	138	109	104	61	34	9	7	6
ee inclusive	12759	9588	7389	7140	5408	1321	411	276	261
ee iso-iso	11797	8990	6907	6681	5146	1186	349	234	220
CMUP-CMUP	2142	1712	1304	1257	970	221	66	48	48
CMUP-NICMUP	174	147	109	101	51	35	15	7	7
CMUP-CMU	862	699	511	495	381	90	24	20	20
CMUP-NICMU	57	50	38	36	18	16	2	1	1
CMUP-CMP	1235	1015	765	737	560	133	44	28	28
CMUP-NICMP	74	64	53	52	26	18	8	3	3
CMUP-CMX	2553	2049	1580	1528	1162	297	69	52	52
CMUP-NICMX	97	79	63	60	29	24	7	4	4
CMX-NICMUP	99	81	60	59	26	22	11	5	5
CMUP-CMIO	943	759	571	542	414	98	30	24	24
CMX-CMX	770	598	449	441	346	82	13	7	7
CMX-NICMX	57	38	32	31	12	15	4	2	2
CMX-CMU	458	376	284	276	222	41	13	9	9
CMX-NICMU	23	20	17	17	4	5	8	5	5
CMX-CMP	646	530	394	375	289	68	18	10	10
CMX-NICMP	26	19	13	12	3	6	3	1	1
CMX-CMIO	468	365	282	268	197	56	15	10	10
mm inclusive	10684	8601	6525	6287	4710	1227	350	236	236
mm iso-iso	10077	8103	6140	5919	4541	1086	292	208	208
CEM-CMUP	7374	7034	5085	4876	3705	916	255	169	168
CEM-NICMUP	371	321	251	248	129	80	39	19	19
CMUP-NICEM	379	300	228	219	109	73	37	24	24
CEM-CMU	1728	1659	1195	1142	892	190	60	35	35
CEM-NICMU	97	82	60	58	30	23	5	2	2
CEM-CMP	2153	2043	1478	1408	1068	267	73	43	42
CEM-NICMP	104	90	78	72	32	28	12	5	5
CEM-CMX	4486	4346	3196	3057	2369	533	155	102	102
CEM-NICMX	228	192	143	133	65	52	16	6	6
CMX-NICEM	197	162	119	114	62	35	17	9	9
CEM-CMIO	1648	1540	1136	1086	851	184	51	25	25
PHX-CMUP	2942	2888	2070	1981	1522	365	94	49	42
PHX-NICMUP	98	93	71	68	30	27	11	6	4
PHX-CMX	1581	1561	1130	1087	854	182	51	31	25
PHX-NICMX	83	77	58	56	20	26	10	3	3
em inclusive	25754	22388	16298	15605	11738	2981	886	528	511
em iso-iso	24113	21071	15290	14637	11261	2637	739	454	439
total inclusive	49197	40577	30212	29032	21856	5529	1647	1040	1008
total iso-iso	45987	38164	28337	27237	20948	4909	1380	896	867

Table 26: PYTHIA WW, `ihht1a`, MC events, after each dilepton cut. The first column represents events with a good dilepton after conversion removal. The last columns gives the final number after all selection cuts.

Category	ALL	Zveto	Met	L-cut	0j	1j	≥2j	Ht	OS
CEM-CEM	15393	3067	2277	2128	687	1101	340	282	230
CEM-NICEM	1929	376	236	198	33	94	71	55	40
PHX-CEM	14098	3097	2388	2217	726	1144	347	271	169
PHX-NICEM	1109	193	112	100	30	32	38	33	23
eee inclusive	32529	6733	5013	4643	1476	2371	796	641	462
eee iso-iso	29491	6164	4665	4345	1413	2245	687	553	399
CMUP-CMUP	4785	1042	760	738	398	254	86	77	70
CMUP-NICMUP	584	126	75	69	13	32	24	15	12
CMUP-CMU	2280	491	375	360	207	127	26	21	20
CMUP-NICMU	121	34	17	16	4	4	8	7	5
CMUP-CMP	2825	603	443	426	256	130	40	37	30
CMUP-NICMP	163	43	27	22	11	7	4	4	4
CMUP-CMX	6259	1335	1017	979	547	336	96	84	66
CMUP-NICMX	360	71	32	29	8	10	11	8	7
CMX-NICMUP	371	64	38	37	15	15	7	6	5
CMUP-CMIO	2150	428	339	328	195	101	32	25	23
CMX-CMX	1878	408	307	299	170	96	33	28	23
CMX-NICMX	194	35	24	22	5	5	12	8	8
CMX-CMU	1219	266	205	200	111	67	22	16	11
CMX-NICMU	73	13	5	4	2	2	0	0	0
CMX-CMP	1478	332	256	241	142	67	32	30	26
CMX-NICMP	104	20	12	12	4	5	3	3	3
CMX-CMIO	1031	192	150	145	74	57	14	12	11
mm inclusive	25875	5503	4082	3927	2162	1315	450	381	324
mm iso-iso	23905	5097	3852	3716	2100	1235	381	330	280
CEM-CMUP	2073	1942	1501	1368	589	589	190	133	65
CEM-NICMUP	166	127	96	84	27	39	18	14	10
CMUP-NICEM	162	106	80	73	19	32	22	15	9
CEM-CMU	468	435	341	311	145	125	41	29	17
CEM-NICMU	38	30	26	23	6	10	7	6	3
CEM-CMP	556	531	427	394	178	157	59	40	24
CEM-NICMP	50	40	31	30	9	12	9	7	5
CEM-CMX	1326	1255	995	912	409	386	117	98	59
CEM-NICMX	84	51	47	40	8	23	9	6	3
CMX-NICEM	102	62	48	44	18	14	12	7	5
CEM-CMIO	489	446	349	313	126	131	56	45	19
PHX-CMUP	1144	1128	884	811	372	322	117	85	44
PHX-NICMUP	70	56	50	42	9	14	19	12	7
PHX-CMX	599	592	446	411	184	173	54	40	21
PHX-NICMX	48	36	28	25	8	11	6	3	1
em inclusive	8256	6837	5349	4881	2107	2038	736	540	292
em iso-iso	7499	6329	4943	4520	2003	1883	634	470	249
total inclusive	66660	19073	14444	13451	5745	5724	1982	1562	1078
total iso-iso	60895	17590	13460	12581	5516	5363	1702	1353	928

Table 27: PYTHIA WZ, `jhht1a`, MC events, after each dilepton cut. The first column represents events with a good dilepton after conversion removal. The last columns gives the final number after all selection cuts.

Category	ALL	Zveto	Met	L-cut	0j	1j	≥2j	Ht	OS
CEM-CEM	18052	3353	1851	1712	1154	369	189	174	153
CEM-NICEM	2628	473	181	150	42	58	50	45	42
PHX-CEM	15194	2412	1281	1193	831	244	118	102	82
PHX-NICEM	1191	196	75	65	22	20	23	14	10
ee inclusive	37065	6434	3388	3120	2049	691	380	335	287
ee iso-iso	33246	5765	3132	2905	1985	613	307	276	235
CMUP-CMUP	6030	1242	689	652	441	139	72	64	61
CMUP-NICMUP	959	217	78	69	18	29	22	18	17
CMUP-CMU	2671	508	293	274	182	67	25	22	21
CMUP-NICMU	200	47	24	23	4	8	11	7	7
CMUP-CMP	3567	708	380	353	241	86	26	24	22
CMUP-NICMP	273	74	22	18	7	8	3	3	3
CMUP-CMX	7021	1321	756	729	491	180	58	51	48
CMUP-NICMX	434	93	29	25	8	8	9	8	8
CMX-NICMUP	412	83	31	29	7	13	9	9	8
CMUP-CMIO	2393	468	270	259	179	56	24	20	19
CMX-CMX	2232	425	216	206	150	38	18	16	14
CMX-NICMX	307	74	23	19	6	12	1	1	1
CMX-CMU	1427	266	151	144	100	26	18	13	12
CMX-NICMU	111	25	8	8	4	4	0	0	0
CMX-CMP	1813	328	192	185	108	58	19	14	14
CMX-NICMP	131	21	10	7	4	2	1	1	1
CMX-CMIO	1229	256	135	127	93	27	7	6	6
mm inclusive	31210	6156	3307	3127	2043	761	323	277	262
mm iso-iso	28383	5522	3082	2929	1985	677	267	230	217
CEM-CMUP	601	555	341	271	50	145	76	67	41
CEM-NICMUP	83	71	36	27	6	9	12	9	7
CMUP-NICEM	74	60	33	29	3	14	12	9	7
CEM-CMU	141	137	73	56	7	34	15	13	11
CEM-NICMU	15	15	6	4	1	2	1	0	0
CEM-CMP	197	180	99	75	14	40	21	16	12
CEM-NICMP	22	17	9	6	1	1	4	3	1
CEM-CMX	342	318	180	150	52	65	33	26	13
CEM-NICMX	36	31	20	14	2	6	6	3	2
CMX-NICEM	29	25	16	11	2	6	3	1	1
CEM-CMIO	146	135	83	67	14	32	21	17	11
PHX-CMUP	264	260	128	100	31	47	22	16	10
PHX-NICMUP	35	35	18	11	1	3	7	4	3
PHX-CMX	156	156	83	67	17	34	16	11	6
PHX-NICMX	14	14	6	3	0	2	1	1	0
em inclusive	2401	2009	1131	891	201	440	250	196	125
em iso-iso	2076	1741	987	786	185	397	204	166	104
total inclusive	70676	14599	7826	7138	4293	1892	953	808	674
total iso-iso	63705	13028	7201	6620	4155	1687	778	672	556

Table 28: PYTHIA ZZ, `khht1a`, MC events, after each dilepton cut. The first column represents events with a good dilepton after conversion removal. The last columns gives the final number after all selection cuts.

Category	ALL	Zveto	Met	L-cut	0j	1j	≥2j	Ht	OS
CEM-CEM	245	24	18	18	15	2	1	1	1
CEM-NICEM	48	6	3	3	2	1	0	0	0
PHX-CEM	269	109	78	68	51	15	2	0	0
PHX-NICEM	22	6	4	4	3	1	0	0	0
ee inclusive	584	145	103	93	71	19	3	1	1
ee iso-iso	514	133	96	86	66	17	3	1	1
CMUP-CMUP	0	0	0	0	0	0	0	0	0
CMUP-NICMUP	0	0	0	0	0	0	0	0	0
CMUP-CMU	0	0	0	0	0	0	0	0	0
CMUP-NICMU	0	0	0	0	0	0	0	0	0
CMUP-CMP	0	0	0	0	0	0	0	0	0
CMUP-NICMP	0	0	0	0	0	0	0	0	0
CMUP-CMX	0	0	0	0	0	0	0	0	0
CMUP-NICMX	0	0	0	0	0	0	0	0	0
CMX-NICMUP	0	0	0	0	0	0	0	0	0
CMUP-CMIO	0	0	0	0	0	0	0	0	0
CMX-CMX	0	0	0	0	0	0	0	0	0
CMX-NICMX	0	0	0	0	0	0	0	0	0
CMX-CMU	0	0	0	0	0	0	0	0	0
CMX-NICMU	0	0	0	0	0	0	0	0	0
CMX-CMP	0	0	0	0	0	0	0	0	0
CMX-NICMP	0	0	0	0	0	0	0	0	0
CMX-CMIO	0	0	0	0	0	0	0	0	0
mm inclusive	0	0	0	0	0	0	0	0	0
mm iso-iso	0	0	0	0	0	0	0	0	0
CEM-CMUP	124	17	13	12	6	4	2	0	0
CEM-NICMUP	24	5	3	3	3	0	0	0	0
CMUP-NICEM	14	2	1	1	1	0	0	0	0
CEM-CMU	42	3	1	1	0	1	0	0	0
CEM-NICMU	1	0	0	0	0	0	0	0	0
CEM-CMP	35	5	4	4	2	1	1	0	0
CEM-NICMP	7	2	2	1	1	0	0	0	0
CEM-CMX	104	19	16	16	10	6	0	0	0
CEM-NICMX	15	0	0	0	0	0	0	0	0
CMX-NICEM	10	0	0	0	0	0	0	0	0
CEM-CMIO	33	2	2	2	1	1	0	0	0
PHX-CMUP	59	59	41	38	31	5	2	0	0
PHX-NICMUP	4	4	3	2	0	2	0	0	0
PHX-CMX	44	44	29	29	23	5	1	0	0
PHX-NICMX	5	5	4	3	1	1	1	0	0
em inclusive	489	149	106	102	73	23	6	0	0
mu iso-iso	569	167	119	112	79	26	7	0	0
total inclusive	1153	312	222	205	150	45	10	1	1
total iso-iso	1003	282	202	188	139	40	9	1	1

Table 29: PYTHIA `Wgamma` MC events, after each dilepton cut. The first column represents events with a good dilepton after conversion removal. The last columns gives the final number after all selection cuts.

Category	ALL	Zveto	Met	L-cut	0j	1j	≥2j	Ht	OS
CEMCEM	1026	892	61	21	3	12	6	2	2
CEMNICEM	156	111	9	4	1	1	2	1	1
PHXCEM	759	657	41	15	3	6	6	3	3
PHXNICEM	69	41	2	0	0	0	0	0	0
ee inclusive	2010	1701	113	40	7	19	14	6	6
ee iso-iso	1785	1549	102	36	6	18	12	5	5
CMUPCMUP	354	335	12	7	1	4	2	2	2
CMUPNICMUP	31	31	3	1	0	0	1	1	1
CMUPCMU	157	148	8	5	0	3	2	1	1
CMUPNICMU	6	6	0	0	0	0	0	0	0
CMUPCMP	189	183	17	6	0	4	2	1	1
CMUPNICMP	10	10	0	0	0	0	0	0	0
CMUPCMX	391	369	23	15	2	4	9	3	3
CMUPNICMX	16	16	2	1	0	1	0	0	0
CMXNICMUP	16	15	0	0	0	0	0	0	0
CMUPCMIO	134	128	13	4	1	2	3	2	2
CMXCMX	132	122	10	5	1	3	1	1	1
CMXNICMX	8	8	0	0	0	0	0	0	0
CMXCMU	84	80	3	1	0	1	0	0	0
CMXNICMU	3	3	0	0	0	0	0	0	0
CMXCMP	85	78	4	2	0	1	1	1	1
CMXNICMP	7	7	0	0	0	0	0	0	0
CMXCMIO	67	64	5	3	0	3	0	0	0
mm inclusive	1690	1603	100	50	5	24	21	12	12
mm iso-iso	1593	1507	95	48	5	23	20	11	11
CEMCMUP	1201	1150	72	34	5	17	12	5	5
CEMNICMUP	60	56	11	2	0	1	1	1	1
CMUPNICEM	73	47	8	5	1	2	2	2	2
CEMCMU	254	240	17	7	0	6	1	0	0
CEMNICMU	7	7	1	1	0	0	1	0	0
CEMCMP	328	316	20	12	1	7	4	3	3
CEMNICMP	17	16	1	0	0	0	0	0	0
CEMCMX	722	700	55	22	2	16	4	3	3
CEMNICMX	32	31	5	3	1	1	1	0	0
CMXNICEM	49	38	2	2	0	0	2	0	0
CEMCMIO	243	367	31	15	0	7	4	4	4
PHXCMUP	366	366	15	4	0	2	2	0	0
PHXNICMUP	21	21	0	0	0	0	0	0	0
PHX_CMU	105	0	0	0	0	0	0	0	0
PHX_NICMU	5	0	0	0	0	0	0	0	0
PHX_CMP	97	0	0	0	0	0	0	0	0
PHX_NICMP	3	0	0	0	0	0	0	0	0
PHXCMX	307	307	16	5	0	3	2	0	0
PHXNICMX	10	10	1	0	0	0	0	0	0
PHXCMIO	115	0	0	0	0	0	0	0	0
em inclusive	4015	3538	244	106	10	60	36	18	18
em iso-iso	3738	3312	215	93	8	56	29	15	15
total inclusive	7715	6842	457	196	22	103	71	36	36
total iso-iso	7116	6368	412	177	19	97	61	31	31

Table 30: PYTHIA $Z \to \tau\tau$, `zewkat`, MC events, after each dilepton cut. The first column represents events with a good dilepton after conversion removal. The last columns gives the number of predicted number.